

September 15, 1999
FINAL REPORT

NEAR FAULT GROUND MOTIONS

Prepared for

PG&E PEER - TASK 5.A

by

Walter Silva
Nick Gregor
Bob Darragh

of

**Pacific Engineering and Analysis
311 Pomona Avenue
El Cerrito, CA 94530**

CONTENTS

Section		Page
1.0	Introduction	1
2.0	Stochastic Finite Fault Model	2
3.0	Earthquakes, Sites, Profiles, and Slip Models	3
4.0	Results of Analyses	4
4.1	Landers Earthquake	4
4.2	Loma Prieta Earthquake	4
4.3	Northridge Earthquake	5
4.4	Imperial Valley Earthquake	5
4.5	Kobe Earthquake	5
5.0	Summary	6
	References	7
Appendix A:	Stochastic Ground Motion Model Description	A-1
	References	A-16
Appendix B:	Site Response Analysis Method	B-1
	References	B-5

LIST OF TABLES

<u>Table Number</u>		<u>Page</u>
1	Earthquakes and Sites	8
2	Landers Crustal Model (from Wald and Heaton, 1994)	14
3	Loma Prieta Crustal Model (from Wald et al., 1991)	15
4	Northridge Crustal Model (from Wald et al., 1996)	16
5	Imperial Valley Crustal Model (from Hartzell and Helmberger, 1982)	17
6	Kobe Regional Velocity Model (from Wald, 1996)	18

LIST OF FIGURES

Figure Number		Page
1	Schematic of Ground Motion Model	19
2	Shallow shear-wave velocity profiles used in modeling the Landers earthquake	20
3	Shallow shear-wave velocity profiles used in modeling the Loma Prieta earthquake	21
4	Shallow shear-wave velocity profiles used in modeling the Northridge earthquake	22
5	Slip model for the Northridge earthquake determined using a single shallow shear-wave velocity profile	23
6	Slip model for the Northridge earthquake determined using rock and soil shallow shear-wave velocity profiles	24
7	Shallow shear-wave velocity profiles used in modeling the Imperial Valley earthquake	25
8	Shallow shear-wave velocity profiles used in modeling the Kobe earthquake	26
9	Median and $\pm 1 \sigma$ amplification factors for 5% damped response spectra computed for generic rock	27
10	Ratio (data/model prediction) of 5% damped response spectra for an average horizontal component at a period of 3 sec versus directivity parameter $X \cos \theta$. Landers earthquake	29
11	Ratio (data/model prediction) of 5% damped response spectra for an average horizontal component at a period of 5 sec versus directivity parameter $X \cos \theta$. Landers earthquake	30

LIST OF FIGURES

<u>Figure Number</u>		<u>Page</u>
12	Ratio (data/model prediction) of 5% damped response spectra for an average horizontal component at a period of 3 sec versus directivity parameter $X \cos \theta$. Loma Prieta earthquake, rise time of 1.5 sec	31
13	Ratio (data/model prediction) of 5% damped response spectra for an average horizontal component at a period of 5 sec versus directivity parameter $X \cos \theta$. Loma Prieta earthquake, rise time of 1.5 sec	32
14	Ratio (data/model prediction) of 5% damped response spectra for an average horizontal component at a period of 3 sec versus directivity parameter $X \cos \theta$. Loma Prieta earthquake, rise time of 0.5 sec	33
15	Ratio (data/model prediction) of 5% damped response spectra for an average horizontal component at a period of 5 sec versus directivity parameter $X \cos \theta$. Loma Prieta earthquake, rise time of 0.5 sec.	34
16	Ratio (data/model prediction) of 5% damped response spectra for an average horizontal component at a period of 3 sec versus directivity parameter $Y \cos \phi$. Northridge earthquake, rise time of 1.4 sec	35
17	Ratio (data/model prediction) of 5% damped response spectra for an average horizontal component at a period of 5 sec versus directivity parameter $Y \cos \phi$. Northridge earthquake, rise time of 1.4 sec	36
18	Ratio (data/model prediction) of 5% damped response spectra for an average horizontal component at a period of 3 sec versus directivity parameter $Y \cos \phi$. Northridge earthquake, rise time of 1.0 sec	37

LIST OF FIGURES

Figure Number		Page
19	Ratio (data/model prediction) of 5% damped response spectra for an average horizontal component at a period of 5 sec versus directivity parameter $Y \cos \phi$. Northridge earthquake, rise time of 1.0 sec	38
20	Ratio (data/model prediction) of 5% damped response spectra for an average horizontal component at a period of 3 sec versus directivity parameter $Y \cos \phi$. Northridge earthquake, rise time of 1.4 sec, slip model derived using shallow rock and soil profiles	39
21	Ratio (data/model prediction) of 5% damped response spectra for an average horizontal component at a period of 5 sec versus directivity parameter $Y \cos \phi$. Northridge earthquake, rise time of 1.4 sec, slip model derived using shallow rock and soil profiles	40
22	Ratio (data/model prediction) of 5% damped response spectra for an average horizontal component at a period of 3 sec versus directivity parameter $Y \cos \phi$. Imperial Valley earthquake	41
23	Ratio (data/model prediction) of 5% damped response spectra for an average horizontal component at a period of 5 sec versus directivity parameter $X \cos \theta$. Imperial Valley earthquake	42
24	Ratio (data/model prediction) of 5% damped response spectra for an average horizontal component at a period of 3 sec versus directivity parameter $X \cos \theta$. Kobe earthquake	43
25	Ratio (data/model prediction) of 5% damped response spectra for an average horizontal component at a period of 5 sec versus directivity parameter $X \cos \theta$. Kobe earthquake	44

2

...

EXECUTIVE SUMMARY

NEAR FAULT GROUND MOTIONS

Pacific Engineering and Analysis

The stochastic finite-fault ground motion model was implemented to validate the ability of the model to predict the effects of rupture directivity on low frequency (< 1 Hz) near source strong ground motions. Validation exercises consisted of examining the ratio (data/model) of average horizontal component 5% damped response spectra versus directivity parameters (Somerville et al., 1997) for oscillator periods of 3 sec and 5 sec. Analyses were performed for five large and well recorded earthquakes: Landers, Loma Prieta, Northridge, Imperial Valley (1979), and Kobe.

Due to constraints in both time and scope, published slip models were used that were largely determined with site (rock or soil) independent shear-wave velocity profiles. These profiles generally have shallow shear-wave velocities that exceed nominal values by factors of 2 and greater, resulting in too little amplification. Using these slip models with realistic shallow generic rock and soil profiles resulted in a large overprediction of motions, even at an oscillator period of 5 sec. Increasing the rise time to produce unbiased motions resulted in unmodeled effects of rupture directivity, that is, poor site specific model performance versus parameters $X \cos \theta$ and $Y \cos \phi$, but good average model performance (zero bias). Using slip model consistent rise times significantly improved model site specific performance (with respect to rupture directivity) but increased model bias significantly. For one earthquake, Northridge, two slip models are available, one based on site independent shallow velocities and one based on site (rock and soil) dependent shallow velocities. Results using the slip model based on site dependent shallow profiles along with a rise time that resulted in zero bias produced a good overall prediction of rupture directivity. These validation exercises suggest that shallow geotechnical profiles may affect the determination of slip models from low frequency (≤ 1 Hz) strong ground motions. Additionally, strong coupling likely exists between source parameters

such as rise time, slip distribution, and rupture velocity along with shallow shear-wave velocities. Rupture directivity effects may be sensitive to these interactions. These results indicate that in order to preserve a strong physical interpretation of source parameters such as rise time, slip distribution, and rupture velocity, appropriately realistic shallow generic rock and soil profiles should be incorporated into source inversions. Additionally, validations and simulations for applications to engineering design practice should include model consistent parameters, accommodating generic site effects that realistically distinguish between rock and soil (shallow geotechnical) site conditions.

NEAR FAULT GROUND MOTIONS

1.0 INTRODUCTION

The original proposal funded under this task was to quantify the effects of near-source ground motions on nonlinear site response and to develop a site response analysis procedure that accommodates differences in fault-normal and fault-parallel low frequency control motions in a manner consistent with observations. This remains an important issue as a potential contradiction exists in having significantly different fault-normal and fault-parallel low-frequency (< 1 Hz) motions and similar high-frequency motions at both rock and soil sites. Typical site response analyses would not preserve these trends at deep soil sites provided they were present in the rock or control motions.

As a result of the recent development of design motions for the San Francisco-Oakland Bay Bridge, issues arose concerning the appropriateness of empirical spectral adjustment factors (Somerville et al., 1997) to accommodate the near-fault effects of rupture directivity. Since the empirical adjustment factors are not well constrained due to the paucity of data for cases where most of the rupture is toward the site in large earthquakes ($M > 7$), numerical modeling provides the only means of assessing their appropriateness. As a result, this project was redirected to validate the stochastic finite-fault ground motion model (Silva et al., 1997), along with two other methodologies, with recordings that display near-source directivity features: an increase (decrease) in low frequency (< 1 Hz) spectral levels for sites with rupture toward the (away from) site relative to average spectral levels over all near-source sites. These trends exist in average horizontal component spectra as well as in fault-normal and fault-parallel component spectra.

Accompanying features in the low frequency time domain that are characteristic for fault-normal and fault-parallel motions include pulse-like motions for rupture toward the site with lower and more oscillatory motions at sites with rupture predominately away from the site. Theoretically, and (in some cases observed), fault normal displacements are expected to be one sided (most of the motion in a single direction) while fault parallel displacements are two (multiple) sided. These time domain features, as well as near-fault response spectral features are also expected to be modulated by relative positions of rupture nucleation, asperity (high slip) locations, and site locations as well as additional geologic noise such as crustal structure variability, non planar faults (e.g., Landers rupture surface), chaotic fault rupture dynamics (variable rise time and rupture velocity), and site effects (1, 2, and 3-D, e.g., Kobe).

As a result of these possible (likely) effects, development of empirical models with few earthquakes and few near-source recordings may be subject to potential bias. Model simulations, with well validated and unbiased models, when averaged over multiple realizations of source, path, and site properties, should provide reliable estimates of the stable features of rupture directivity. If models provide unbiased estimates of currently available near-source records which display directivity features, confidence is gained in exercising the models for ranges in

conditions (source size and site location) not reflected in the current strong motion data set which impacts engineering design practice.

The validation exercise is intended to evaluate the model's capability to match the response spectral and time domain trends displayed in near-fault recorded motions using a suite of "goodness of fit" parameters.

In our implementation of the stochastic finite-fault model, near surface (top 100-1,000 ft) materials are considered in detail through an equivalent-linear formulation (Appendix B). These shallow profiles are generally neglected in seismological determinations of slip models using recordings of strong ground motion. Since we were unable to develop slip models that incorporate the effects of shallow materials due to insufficient time and scope, we relied on published slip distributions. The anticipated effect was obvious, a general large overprediction of motions. As a result, our validation did not include fault-normal and fault-parallel response spectral and time domain analyses.

Due to the implied importance of near-surface materials (site response) in low frequency strong ground motions, slip models should be determined that are consistent with the shallow rock and soil site conditions that exist at recording sites. Additionally, the coupling that exists between source parameters such as slip distribution, rise time, and rupture velocity further emphasize the importance of determining consistent model parameters for use in modeling cases for which no data exist: very large earthquakes at close site distances. That is, even when very rigorous seismological models are used to infer source parameters, neglecting important amplification effects in the recorded motions due to site response compromises the physical interpretation of source parameters such as rise time, slip distribution, and rupture velocity. This can result in considerable ambiguity in applications to future earthquakes as the unmodeled site effects have likely been incorporated into source parameters. Additionally, for simulation methodologies that do not accommodate rock and soil site effects in validations, a similar ambiguity exists in how the simulated motions are to be treated in design practice: do they represent rock or soil site motions and should they be used in site response analyses for applications to soil sites.

2.0 STOCHASTIC FINITE-FAULT MODEL

The stochastic finite-fault model implemented here is quite simple in concept, using a single-corner-frequency omega-square source spectrum ($M = 5.0$) for each subfault. Large earthquakes are simulated by simply delaying and summing contributions from the $M 5$ subfaults. The process is depicted schematically in Figure 1 and discussed in detail in Appendix A. The model is simple, includes a frequency domain random vibration theory equivalent-linear site response (Appendix B) implemented for both rock and soil sites (Silva et al., 1997). The model, including site effects, has recently been validated at about 500 sites for 15 earthquakes ($M 5.2$ to 7.4) over fault distances ranging from 1 km to 470 km (Silva et al., 1997) and for subduction zone earthquakes for M up to 8.1. In general, the model is unbiased over the frequency range of recorded motions (spectral acceleration averaging from about 0.3 to 100 Hz).

3.0 EARTHQUAKES, SITES, PROFILES, AND SLIP MODELS

Five large and well recorded earthquakes were modeled in this exercise: 1992 M 7.3 Landers, 1989 M 6.9 Loma Prieta, 1994 M 6.7 Northridge, 1979 M 6.5 Imperial Valley, and the 1995 M 6.9 Kobe. The recording sites are those within about 30 km of the rupture surface and are listed in Table 1 along with their directivity parameters (Somerville et al., 1997). To illustrate the differences in the shallow shear-wave velocity profiles, Figures 2-4 and 7-8 show the generic rock and soil profiles used in the current modeling exercises along with those used to determine the slip models.

For the Landers earthquake, the slip model of Wald and Heaton (1994) was used and Figure 2 shows the large difference in shallow shear-wave velocities between generic rock and soil profiles and the site independent shear-wave velocity used in determining the slip model. The difference in amplification between the two is large, about a factor of three, resulting in a large overprediction in ground motions (next Section).

The Loma Prieta profiles are shown in Figure 3 and the slip model used is from Wald et al., 1991. In this case, the shallow shear-wave velocity used in determining the slip model is lower than at Landers (1 km/sec compared to 1.8 km/sec, see Tables 2 and 3). The difference in amplification is still large however, about a factor of 2.

For the Northridge earthquake, two slip models are available, one using a single profile for rock and soil sites (Wald and Heaton, 1994) and one determined using separate rock and soil site profiles (Wald et al., 1996) (Figure 4). The two slip models are shown in Figures 5 and 6 respectively. Although the pattern in overall slip is similar between the two inversions, the two zones of high slip (large asperities) have different amplitudes and have moved both absolutely as well as relative to each other. Additionally, resulting rise times are somewhat different as expected (Wald et al., 1996). The different slip models result in different directivity effects (next Section), suggesting the importance of incorporating more realistic shallow velocities in source inversions.

The Imperial Valley earthquake profiles are shown in Figure 7 and the slip model is from Hartzell and Helmberger (1982). In this case only soil sites were used in the source inversion and the shallow profile is at 700 m/sec (top 105m) which is much greater than the measured values across the El Centro Array from which the generic profile was developed (Figure 7).

In the final earthquake, Kobe, three soil profiles and one rock profile were used (Figure 8) in the modeling. A slip model developed by Wald et al. (1996), using separate rock and soil profiles (Figure 8), resulted in a large broad-band underprediction at all sites. Significantly better results were found using a more compact slip model which was based on empirical (aftershock) Green functions (Kamae and Irikura, 1998). Any 2D and 3D effects due to the basin edge on the recorded motions for both the main shock and empirical Green functions should be appropriately accommodated. Since we do not include these effects in our 1D profiles, an apparent contradiction may exist (providing the basin edge effects are significant at the recording stations used in determining the slip model). This further emphasized the importance of using model consistent parameters and should be evaluated by determining slip

models with both 1D and 3D structures.

To illustrate the potential differences in amplification between the generic shallow rock and soil profiles used here and the site independent profiles used in developing the slip models, Figure 9 shows median and $\pm 1 \sigma$ amplification factors for 5% damped response spectra. These amplification factors are computed for the Los Angeles area (Northridge earthquake) and are given relative to the site independent profile (Figure 4, 1 km/sec). They are keyed to the expected rock outcrop (1 km/sec) PGA values to accommodate nonlinear response effects. At low frequency (< 1 Hz) the generic rock amplification shows a deamplification (0.7 to 0.9) while the deep generic soil show an amplification of about 50%. These differences may then be projected into the source parameters if a single high velocity (1 km/sec) profile is used in the source inversions.

4.0 RESULTS OF ANALYSES

Analyses consisted of examining the ratio (data to model) of average (log) horizontal component 5% damped response spectra plotted as functions of directivity parameters $X \cos \theta$ and $Y \sin \phi$ in (Somerville et al., 1997) Table 1. Oscillator periods of both 3 sec and 5 sec are analyzed.

4.1 Landers Earthquake

Figure 10 shows the $S_a(\text{data})/S_a(\text{model})$ at an oscillator period of 3 sec versus $X \cos \theta$. If there are no trends in the data with the directivity parameter and the ratios are near 1, the model is capturing the observed features of directivity and is unbiased. In general the trend is reasonably flat but in the range of 0.1 to 0.3, indicating that the model captures directivity effects but is dramatically overpredicting the recorded motions. The difference in the shallow profiles between the generic rock and soil used in the validation exercise and the very stiff (1.8 km/sec, Figure 2) profile used in determining the slip model is likely causing the difference.

For a period of 5 sec, Figure 11 shows the corresponding results. The trend is similar and nearly flat except for 1 site at $X \cos \theta$ near 0.9.

4.2 Loma Prieta Earthquake

Figures 12 and 13 shows the 3 sec and 5 sec oscillator results respectively for the Loma Prieta earthquake. In this case the trends (slope) in the ratios indicate that the model is not capturing directivity effects. The average levels indicate that the model is underpredicting as well (particularly at 5 sec). In this case a rise time of 1.5 sec was used which gave largely unbiased predictions over all sites, near-source and distant (out to about 80 km), and over a wide frequency range (0.3 to 100 Hz). Reducing the source rise time to 0.5 sec to be consistent with that obtained in the slip model inversion gave the results shown in Figures 14 and 15. With the

reduced rise time, the trend (slope) is significantly reduced accompanied with a marked overprediction. Interestingly these results imply that rise time is important not only in overall spectral levels but in directivity effects as well. Since source rise times are poorly resolved and highly variable, these results indicate that directivity effects may be highly variable as well. Rise times, directivity effects, and shallow geotechnical properties are likely strongly coupled parameters.

4.3 Northridge Earthquake

For the Northridge earthquake, due to its shallow dip, analyses were done only for the $Y \cos \phi$ directivity parameter. For the rise time that results in unbiased motions (1.4 sec), Figures 16 and 17 show the ratios of data to model predictions for 3 sec and 5 sec respectively using the slip model determined with the site independent shallow velocity profile (figure 5). The results show a trend, particularly for $Y \cos \phi$ values above 0.75. As with the Loma Prieta earthquake, reducing the rise time to a value more consistent with that obtained in the inversions to obtain the slip model (1.0 sec) shows a significant reduction in slope with the accompanying overprediction (Figures 18 and 19).

If a slip model is used that results from different shallow rock and soil site profiles (Figure 6) along with the rise time that results in zero bias (1.4 sec), the trends in $Y \cos \phi$ are largely absent (Figures 20 and 21). As with the Loma Prieta earthquake, these results suggest the importance of the shallow profiles along with coupling between rise time, slip model, and site dynamic material properties.

4.4 Imperial Valley Earthquake

Figures 22 and 23 show the 3 sec and 5 sec results for the Imperial Valley earthquake using the generic El Centro Array profile (Figure 7). The expected overprediction is seen (on average) with little overall trend as $Y \cos \theta$ increases. In general the model is capturing most of the directivity variations.

4.5 Kobe Earthquake

For the Kobe earthquake, the directivity results are shown in Figures 24 and 25 for 3 sec and 5 sec respectively. In this case, using the slip model based on empirical Green functions and a rise time that results in unbiased motions, a general trend is seen in both Figures but only for soil sites. The model is not completely accommodating directivity effects for soil sites but appears to perform reasonably well for rock sites, although the number of rock sites is small. This may be related to basin edge effects incorporated in determining the slip model but neglected in the use of 1D site profiles. This would not be expected to affect rock sites.

5.0 SUMMARY

The stochastic finite-fault ground motion model was implemented to validate the ability of the model to predict the effects of rupture directivity on low frequency (< 1 Hz) near source strong ground motions. Validation exercises consisted of examining the ratio (data/model) of average horizontal component 5% damped response spectra versus directivity parameters (Somerville et al., 1997) for oscillator periods of 3 sec and 5 sec. Analyses were performed for five large and well recorded earthquakes: Landers, Loma Prieta, Northridge, Imperial Valley (1979), and Kobe.

Due to constraints in both time and scope, published slip models were used that were largely determined with site (rock or soil) independent shear-wave velocity profiles. These profiles generally have shallow shear-wave velocities that exceed nominal values by factors of 2 and greater, resulting in too little amplification. Using these slip models with realistic shallow generic rock and soil profiles resulted in a large overprediction of motions, even at an oscillator period of 5 sec. Increasing the rise time to produce unbiased motions resulted in unmodeled effects of rupture directivity, that is, poor site specific model performance versus parameters $X \cos \theta$ and $Y \cos \phi$, but good average model performance (zero bias). Using slip model consistent rise times significantly improved model site specific performance (with respect to rupture directivity) but increased model bias significantly. For one earthquake, Northridge, two slip models are available, one based on site independent shallow velocities and one based on site (rock and soil) dependent shallow velocities. Results using the slip model based on site dependent shallow profiles along with a rise time that resulted in zero bias produced a good overall prediction of rupture directivity. These validation exercises suggest that shallow geotechnical profiles may affect the determination of slip models from low frequency (≤ 1 Hz) strong ground motions. Additionally, strong coupling likely exists between source parameters such as rise time, slip distribution, and rupture velocity along with shallow shear-wave velocities. Rupture directivity effects may be sensitive to these interactions. These results indicate that in order to preserve a strong physical interpretation of source parameters such as rise time, slip distribution, and rupture velocity, appropriately realistic shallow generic rock and soil profiles should be incorporated into source inversions. Additionally, validations and simulations for applications to engineering design practice should include model consistent parameters, accommodating generic site effects that realistically distinguish between rock and soil (shallow geotechnical) site conditions.

REFERENCES

- Hartzell, S.H., and Helmberger, D.V. (1982). "Strong-motion modeling of the Imperial Valley earthquake of 1979." *Bull. Seism. Soc. Am.*, 72(2), 571-596.
- Kamae, K. and K. Irikura (1998). "Source model of the 1995 Hyogo-ken Nanbu earthquake and simulation of near-source ground motion." *Bull. Seism. Soc. Am.*, 88(2), 400-412.
- Liu, H-L, and Helmberger, D.V. (1985). "The 23:19 aftershock of the 15 October 1979 Imperial Valley Earthquake: More evidence for an asperity." *Bull. Seism. Soc. Am.*, 75(3), 689-708.
- Silva, W.J., N. Abrahamson, G. Toro, C. Costantino (1997). "Description and validation of the stochastic ground motion model." Submitted to Brookhaven National Laboratory, Associated Universities, Inc. Upton, New York.
- Somerville, P.G., Smith, N.F., Graves, R.W. and Abrahamson, N.A. (1997). "Modification of empirical strong ground motion attenuation relations to include the amplitude and duration effects of rupture directivity." *Seism. Resear. Lett.*, 68(1), 199-222.
- Wald, D.J. (1996). "Slip history of the 1995 Kobe, Japan, earthquake determined from strong motion, teleseismic, and geodetic data." *J. of Physics of the Earth*, in press.
- Wald, D.J., T.H. Heaton and K.W. Hudnut (1996). "The slip history of the 1994 Northridge, California, earthquake determined from strong-motion, teleseismic, GPS, and leveling data." *Bull. Seism. Soc. Am.*, 86(1B), S49-S70.
- Wald, D.J., Heaton, T.H. (1994). "Spatial and temporal distribution of slip for the 1992 Landers, California, earthquake." *Bull. Seism. Soc. Amer.*, 84(3), 668-691.
- Wald, D.J., D.V. Helmberger, and T.R. Heaton (1991). "Rupture model of the 1989 Loma Prieta Earthquake from the inversion of strong motion and broadband teleseismic data." *Bull. Seism. Soc. Amer.*, 81(5), 1540-1572.

Table 1
EARTHQUAKES AND SITES

Earthquake	Mag	Station Name	Condition	Closest to Rupture (km)	X*cos(theta)	Y*cos(phi)
Landers 06/28/92	7.3	Barstow	rock	35.41*	0.79194	0.09113
		Coolwater	rock	19.15*	0.85274	0.16137
		Desert Hot Springs	rock	22.77	0.06559	0.13812
		Fort Irwin	rock			
		Joshua Tree	rock	10.60	0.04554	0.25900
		Lucerne	rock	4.67*	0.58240	0.39102
		Morongo Valley	rock	18.37	0.05051	0.16736
		North Palm Springs	rock	27.85	0.06404	0.11458
		Palm Springs Airport	soil	36.84	0.06790	0.08775
		Yermo Fire Station	soil	21.80*	0.87491	0.14368
		Loma Prieta 10/18/89	6.9	Agnews State Hospital	soil	24.52
Anderson Dam (Downstream)	rock			20.05	0.08010	0.79733
Anderson Dam, L Abut	rock			19.99	0.07972	0.79749
APEEL #2 Redwood City	soil			43.86	0.45984	0.56298
APEEL 7 - Pulgas	rock			42.19	0.48348	0.49742
APEEL 9 - Crystal Springs Res	rock			41.00	0.48746	0.48587
APEEL 10 - Skyline	rock			41.92	0.49068	0.46257
Belmont - Envirotech	rock			44.06	0.48010	0.50078
BRAN	rock			10.72	0.15820	0.70134
Capitola	soil			15.02	0.00029	0.48239
Corralitos	rock			3.85	0.09555	0.82318
Coyote Lake Dam (Downstr)	rock	20.83	0.24998	0.79516		

Table 1 (cont.)
EARTHQUAKES AND SITES

Earthquake	Mag	Station Name	Condition	Closest to Rupture (km)	X*cos(theta)	Y*cos(phi)
		Coyote Lake Dam (SW Abut)	rock	20.37	0.26355	0.79643
		Gilroy Gavilan College	rock	10.02	0.46029	0.80453
		Gilroy, Historic Bldg	soil	11.02	0.42944	0.81560
		Gilroy #1	rock	9.69	0.46093	0.80639
		Gilroy #2	soil	11.13	0.45178	0.80294
		Gilroy #3	soil	12.88	0.44523	0.79528
		Gilroy #4	soil	14.52	0.42876	0.79495
		Gilroy #6	rock	18.38	0.40777	0.78297
		Gilroy #7	soil	22.73	0.40052	0.76185
		Hollister City Hall	soil	27.42	0.48940	0.57927
		Hollister Differential Array	soil	24.86	0.48075	0.63516
		Hollister-South & Pine	soil	27.96	0.48961	0.57322
		LGPC	rock	3.87	0.43623	0.82200
		Palo Alto - 1900 Embarcadero	soil	30.74	0.44127	0.67208
		Palo Alto - SLAC	soil	30.50	0.47620	0.60166
		Salinas - John & Work	soil	32.65	0.45549	0.05056
		Saratoga-Aloha	rock	8.49	0.46008	0.81511
		Saratoga WVC	rock	9.30	0.44359	0.81911
		Sunnyvale - Colton Ave	soil	24.18	0.41127	0.74575
		UCSC	rock	18.54	0.14161	0.29339
		Santa Cruz UCSC/Lick Observator	rock	6.55	0.00605	0.78483
		UCSC WAHO	soil	17.39	0.02015	0.35127

Table 1 (cont.)
EARTHQUAKES AND SITES

Earthquake	Mag	Station Name	Condition	Closest to Rupture (km)	X*cos(theta)	Y*cos(phi)
		Woodside	rock	34.06	0.48446	0.54606
Northridge 01/17/94	6.7	Arleta - Nordhoff Fire Sta	rock	8.63	0.14256	0.68047
		Big Tujunga, Angeles Nat F	rock	19.75	0.14586	0.72062
		Brentwood V.A. Hospital	rock	22.42	0.19035	0.02212
		Burbank - Howard Rd.	rock	16.92	0.18772	0.65704
		Canoga Park - Topanga Can	soil	14.66	0.22876	0.22832
		Canyon Country - W Lost Cany	soil	12.45	0.01461	0.80876
		Castaic - Old Ridge Route	rock	20.66	0.53711	0.75816
		Glendale - Las Palmas	soil	22.22	0.18901	0.61886
		Jensen Filter Plant	soil	5.42	0.01333	0.79083
		LA Dam	rock	5.66	0.00447	0.78775
		LA - Wonderland Ave	rock	20.22	0.22000	0.23429
		La Crescenta - New York	soil	18.56	0.17017	0.68383
		Lake Hughes 9	rock	25.29	0.41886	0.77920
		Lake Hughes 12A	rock	21.30	0.42242	0.78801
		N. Hollywood - Coldwater Can	rock	12.46	0.19699	0.53825
		Newhall - Fire Sta	soil	6.16	0.21809	0.80753
		Newhall - W. Pico Canyon Rd.	rock	6.00	0.21296	0.80714
		Northridge - 17645 Saticoy St	soil	12.05	0.11798	0.40767
		Pacoima Dam (downstr)	rock	7.03	0.05181	0.80852

Table 1 (cont.)
EARTHQUAKES AND SITES

Earthquake	Mag	Station Name	Condition	Closest to Rupture (km)	X*cos(theta)	Y*cos(phi)
		Pacoima Kagel Canyon	rock	7.40	0.10673	0.78953
		Pardee - SCE Substation	soil	7.45	0.47818	0.80811
		Rinaldi Receiving Sta	soil	6.51	0.01053	0.77803
		Santa Susana Ground	rock	16.87	0.71808	0.10619
		Sepulveda VA	soil	8.41	0.07582	0.66128
		Simi Valley - Katherine Rd	soil	13.44	0.68000	0.30903
		Stone Canyon	rock	19.01	0.20898	0.11400
		Sun Valley - Roscoe Blvd	soil	9.98	0.16823	0.64198
		Sunland - Mt Gleason Ave	rock	13.38	0.14468	0.74483
		Sylmar - Converter Sta South	soil	5.18	0.00163	0.79427
		Sylmar - Converter Sta East	soil	5.34	0.00642	0.79180
		Sylmar - Olive View Med FF	soil	5.30	0.00813	0.80432
		Topanga - Fire Sta	rock	22.21	0.05014	-0.00260
		Vasquez Rocks Park	rock	23.61	0.00115	0.79679
Imperial Val. 10/15/79	6.5	Aeropuerto Mexicali	soil	1.24	0.04236	0.99235
		Agrarias	soil	1.02	0.04678	0.99479
		Bonds Corner	soil	1.11	0.15733	0.99383
		Brawley Airport	soil	10.13	0.93342	0.70103
		Calexico Fire Sta.	soil	12.01	0.23874	0.63837
		Calipatria Fire Sta.	soil	25.27	0.90907	0.36666

Table 1 (cont.)
EARTHQUAKES AND SITES

Earthquake	Mag	Station Name	Condition	Closest to Rupture (km)	X*cos(theta)	Y*cos(phi)
		Cerro Prieto	rock	23.20	0.04080	0.39442
		Chihuahua	soil	16.94	0.04783	0.50679
		Cucupah	soil			
		El Centro - Imp County Center	soil	8.97	0.68449	0.74303
		El Centro - Meloland Overpass	soil	1.71	0.50801	0.98564
		El Centro #1	soil	20.33	0.61104	0.43994
		El Centro #2	soil	13.88	0.64187	0.58283
		El Centro #3	soil	11.37	0.63277	0.65882
		El Centro #4	soil	5.48	0.68538	0.87597
		El Centro #5	soil	2.34	0.72736	0.97342
		El Centro #6	soil	0.29	0.71996	0.99957
		El Centro #7	soil	2.23	0.71763	0.97580
		El Centro #8	soil	5.53	0.70580	0.87445
		El Centro #10	soil	10.21	0.65359	0.69817
		El Centro #11	soil	14.10	0.59600	0.57700
		El Centro #12	soil	19.59	0.52023	0.45321
		El Centro #13	soil	23.63	0.53332	0.38848
		El Centro Diff Array, Dogwood	soil	6.75	0.66823	0.82777
		Holtville Post Office	soil	6.13	0.46573	0.85173
		Parachute Test Site	rock	15.16	0.92889	0.54917
		Plaster City	soil	32.46	0.77293	0.29337
		SAHOP Casa Flores	soil	10.62	0.04652	0.68404
		Superstition Mountain	rock	27.10	0.90678	0.34497
		Westmorland	soil	16.79	0.94868	0.51024

**Table 1 (cont.)
EARTHQUAKES AND SITES**

Earthquake	Mag	Station Name	Condition	Closest to Rupture (km)	X*cos(theta)	Y*cos(phi)
Kobe 01/16/95	6.9	Abeno	soil	24.81	0.52820	0.82467
		Amagasaki	soil	11.31	0.57551	0.86624
		Chihaya	rock	49.81	0.31692	0.77030
		Fukushima	soil	17.82	0.58211	0.84552
		Kakogawa	soil	19.27*	0.00489	0.34163
		Kobe University	rock	0.85	0.41818	0.88987
		KJMA	rock	0.45	0.30828	0.88999
		Morigawachi	soil	24.78	0.58273	0.82076
		Nishi-Akashi	soil	7.04*	0.00527	0.77627
		OSAJ	soil	21.33	0.58741	0.83434
		Port Island (0m)	soil	3.21	0.30042	0.88738
		Port Island (16m)		3.21	0.30042	0.88738
		Port Island (32m)	soil	3.21	0.30042	0.88738
		Port Island (83m)	soil	3.21	0.30042	0.88738
		Sakai	soil	27.99	0.35565	0.81606
		Shin-Osaka	soil	16.96	0.62491	0.84247
		Tadoka	soil	31.53	0.16843	0.80701
Takarazuka	soil	0.28	0.63961	0.88994		
Takatori	soil	1.35	0.20488	0.88958		
Yae	soil	27.77	0.57877	0.80818		

NOTES:

For the San Fernando earthquake all the distances are to the closest idealized rupture plane. The distances with a * are to the San Fernando rupture plane. The distances without a * are to the Sierra Madre rupture plane.

For the Landers earthquake all the distances are to the closest idealized rupture plane. The distances with a * are to the Camp Rock rupture plane. The distances without a * are to the Johnson Valley rupture plane.

For the Kobe earthquake all the distances are to the closest idealized rupture plane. The distances with a * are to the Nojima rupture plane. The distances without a * are to the Suma/Suwayama rupture plane.

Table 2
LANDERS CRUSTAL MODEL
(from Wald and Heaton, 1994)

Thickness (km)	V_p (km/sec)	Density (cgs)
1.5	1.98	2.30
2.5	3.15	2.60
22.0	3.52	2.70
5.0	3.83	2.87
	4.50	3.10

Table 3
LOMA PRIETA CRUSTAL MODEL
(from Wald et al., 1991)

Thickness (km)	V_p (km/sec)	Density (cgs)
0.1	1.00	2.00
0.4	1.95	2.30
0.5	2.48	2.35
2.0	2.77	2.35
2.0	3.10	2.35
2.0	3.31	2.45
2.0	3.55	2.58
4.0	3.61	2.62
5.0	3.62	2.63
7.0	3.85	2.77
	4.62	3.28

Table 4
NORTHRIDGE CRUSTAL MODEL
 (from Wald et al., 1996)

Rock Sites		
Thickness (km)	V_s (km/sec)	Density (cgs)
0.5	1.0	2.1
1.5	2.0	2.3
2.5	3.2	2.5
23.0	3.6	2.6
13.0	3.9	2.9
---	4.5	3.0
Soil Sites		
Thickness (km)	V_s (km/sec)	Density (cgs)
0.1	0.3	1.7
0.2	0.5	1.8
0.2	1.0	2.1
1.0	2.0	2.4
2.5	3.2	2.7
23.0	3.6	2.8
13.0	3.9	2.9
---	4.5	3.3

Table 5
IMPERIAL VALLEY CRUSTAL MODEL
 (from Hartzell and Helmberger, 1982)

Thickness (m)	V_s (m/sec)	Density (cgs)
105.00	700.00	1.74
105.00	800.00	1.85
105.00	900.00	1.89
105.00	1000.00	1.94
105.00	1150.00	2.03
105.00	1300.00	2.15
339.00	1500.00	2.26
480.00	1640.00	2.36
160.00	1740.00	2.39
160.00	1910.00	2.44
160.00	2080.00	2.48
160.00	2150.00	2.50
640.00	2220.00	2.52
160.00	2300.00	2.55
160.00	2500.00	2.60
160.00	2710.00	2.63
2271.00	2750.00	2.65
5000.00	3180.00	2.75
10000.00	4100.00	2.80
0.00	4500.00	3.20

**Table 6
 KOBE REGIONAL VELOCITY MODEL
 (from Wald, 1996)**

Rock Sites		
Thickness (km)	V_s (km/sec)	Density (cgs)
0.10	1.00	2.10
0.40	1.80	2.10
4.50	3.20	2.60
22.00	3.46	2.70
5.00	3.83	2.87
	4.50	3.50
Soil Sites		
Thickness (km)	V_s (km/s)	Density (g/cm³)
0.10	0.30	1.70
0.10	0.50	1.82
1.00	1.00	2.10
0.40	1.80	2.10
4.50	3.20	2.60
20.90	3.46	2.70
5.00	3.83	2.87
	4.50	3.50

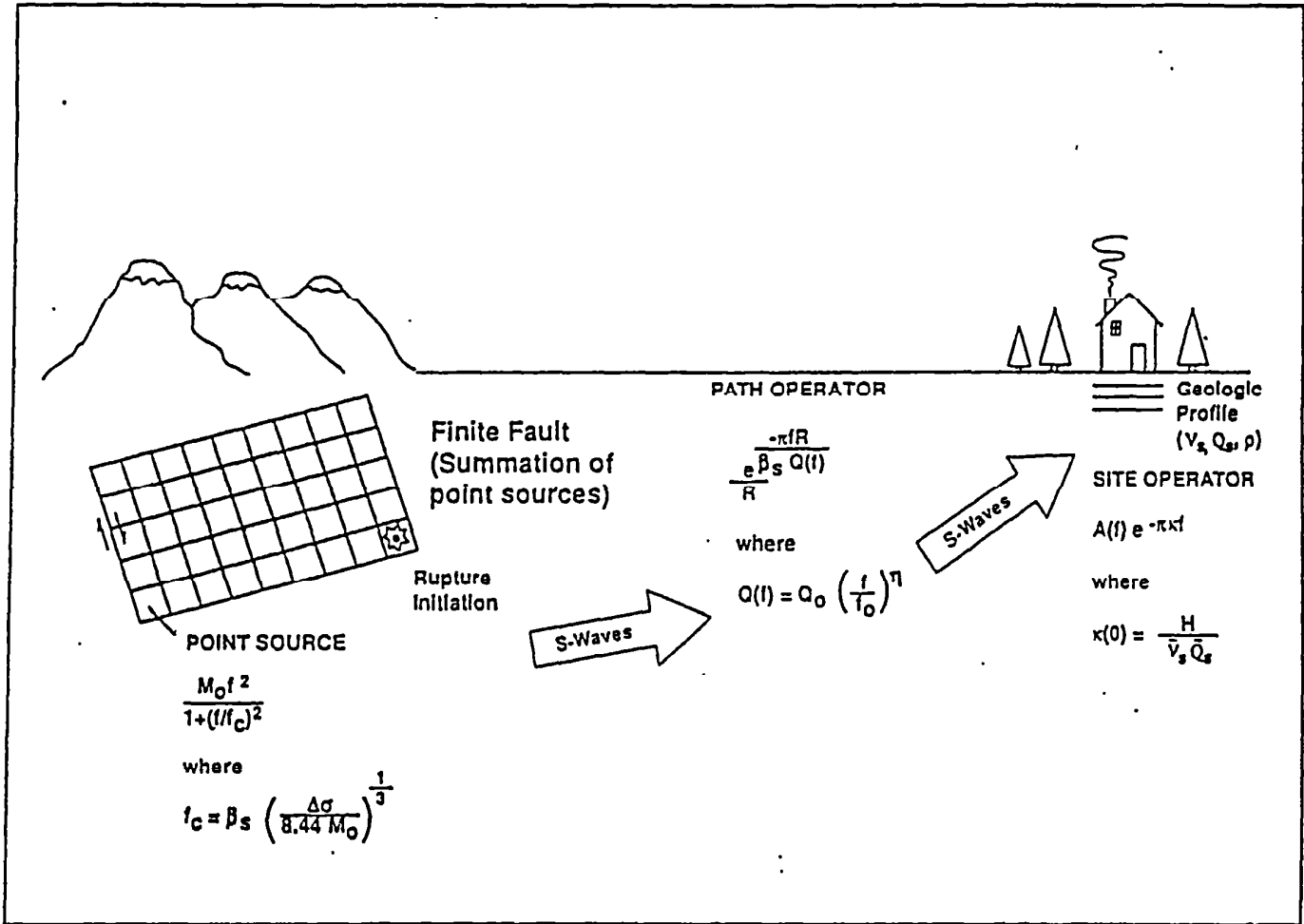
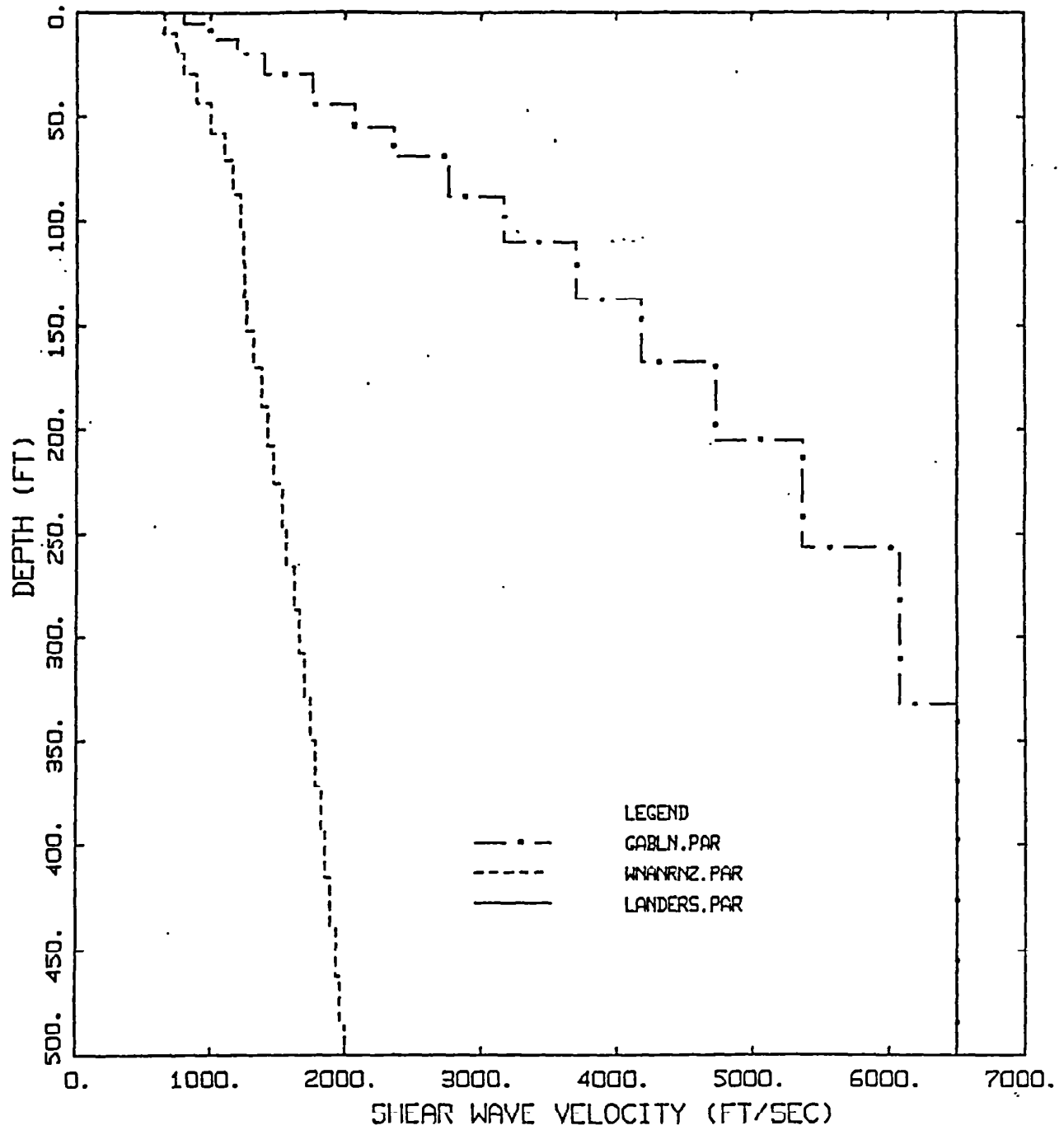
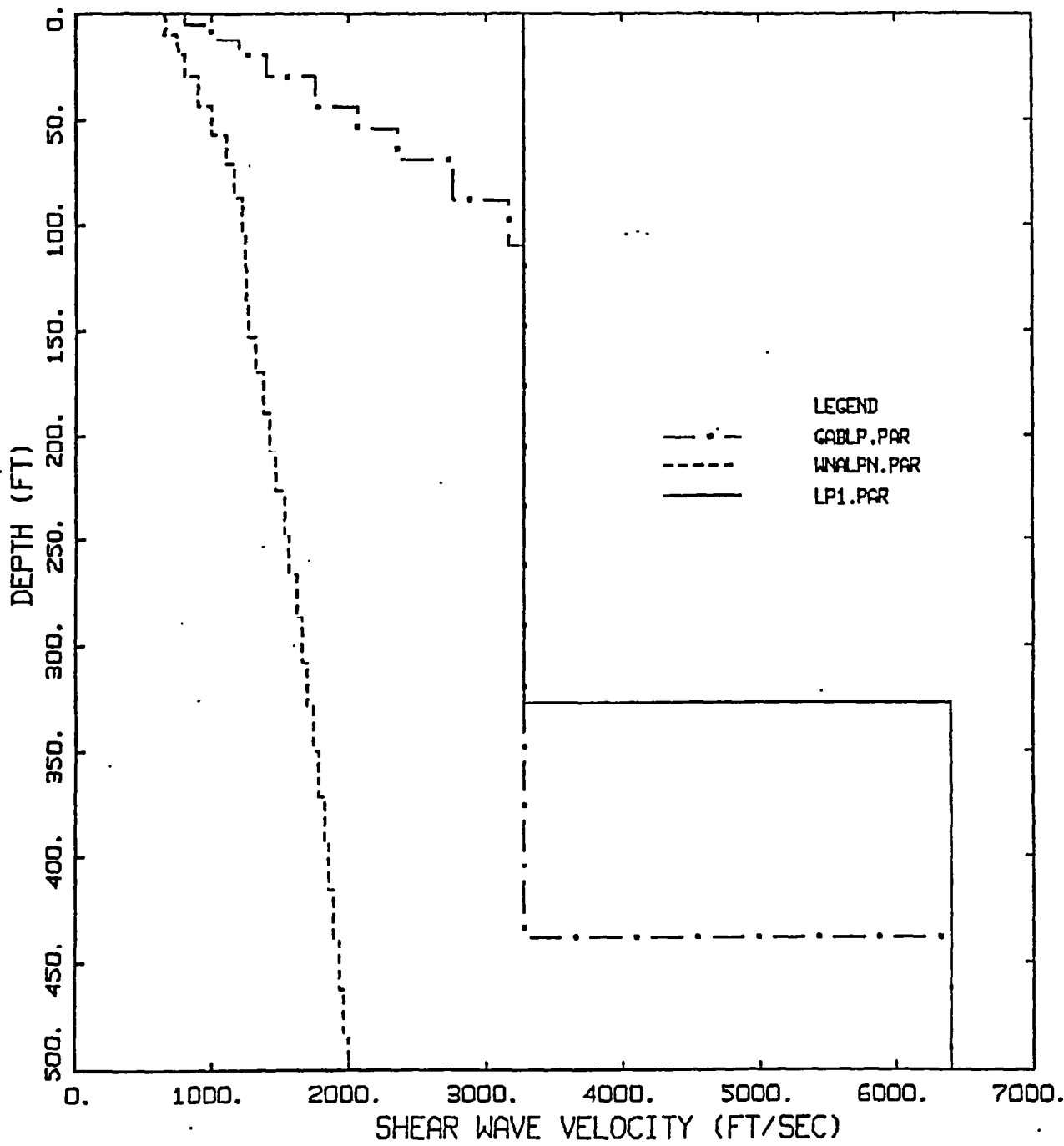


Figure 1. Schematic of ground motion model.



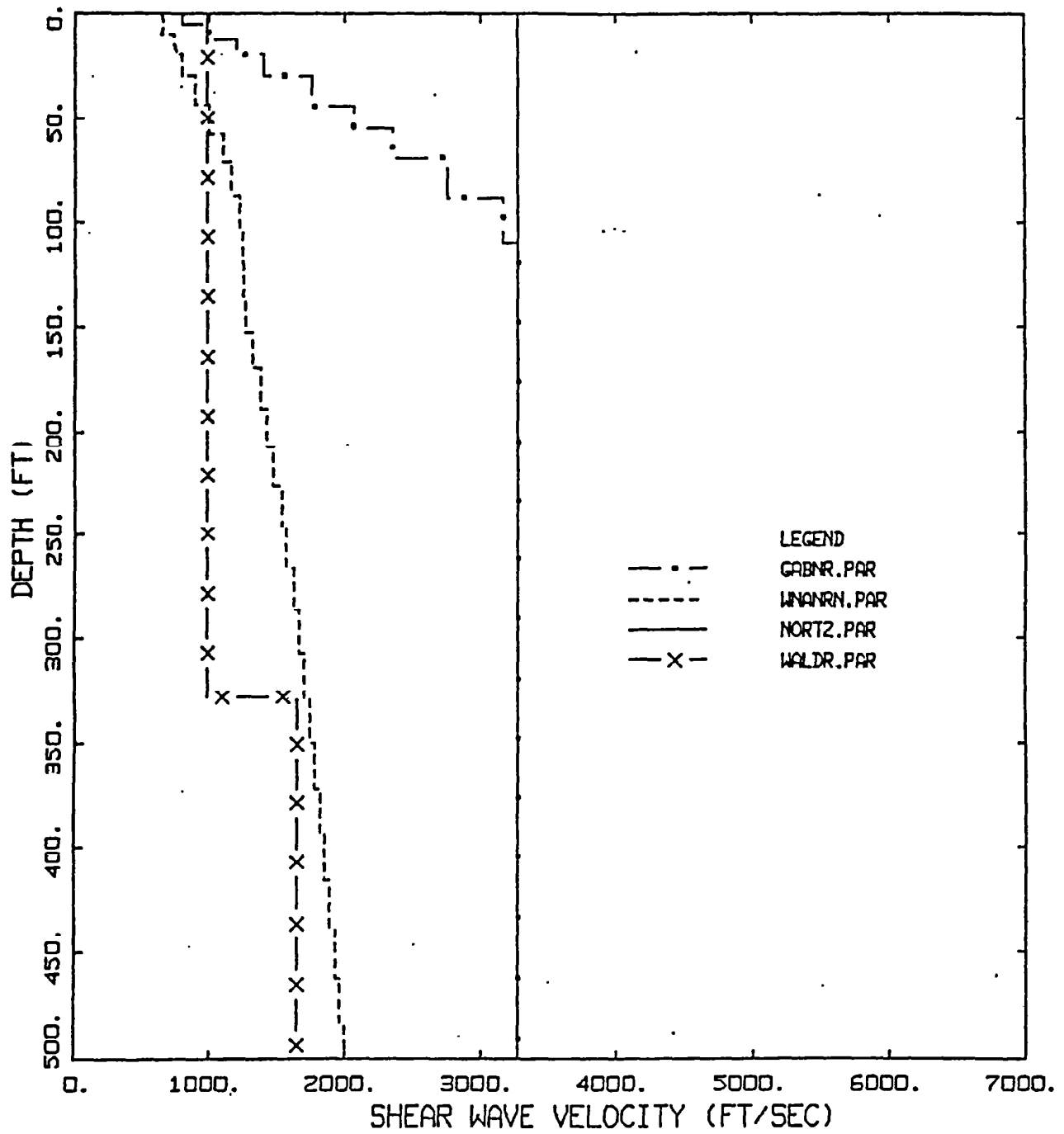
SHEAR WAVE VELOCITY PROFILE LANDERS PROFILES

Figure 2. Shallow shear-wave velocity profiles used in modeling the Landers earthquake (rock, dash dotted; soil, dashed) and in determining the slip model (rock and soil, solid) (Table 2).



SHEAR WAVE VELOCITY PROFILE
 LOMA PRIETA PROFILES

Figure 3. Shallow shear-wave velocity profiles used in modeling the Loma Prieta earthquake (rock, dash dotted; soil, dashed) and in determining the slip model (rock and soil, solid) (Table 3).



SHEAR WAVE VELOCITY PROFILE NORTHRIDGE PROFILES

Figure 4. Shallow shear-wave velocity profiles used in modeling the Northridge earthquake (rock, dash dotted; soil, dashed) and in determining the slip model (rock, solid; dash crosses, soil) (Table 4).

Northridge Earthquake Strong Motion Slip

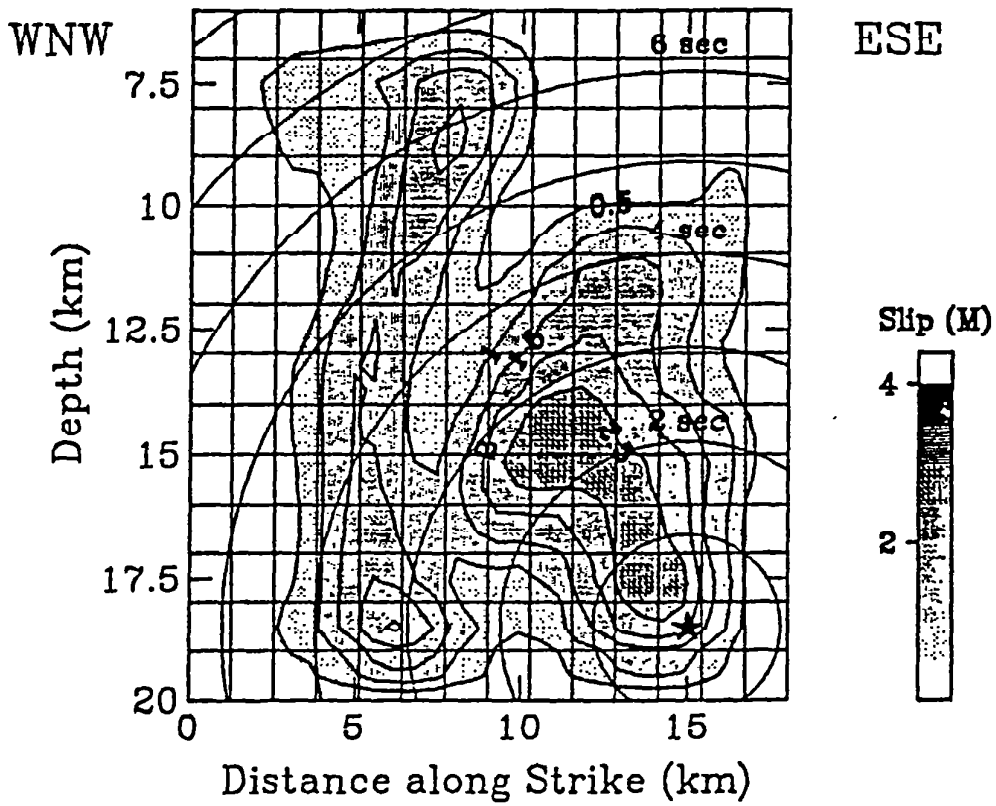


Figure 5. Slip model for the Northridge earthquake determined using a single shallow shear-wave velocity profile (1 km/sec, Figure 4). Source, Wald and Heaton, 1994.

Northridge Earthquake Strong Motion Slip

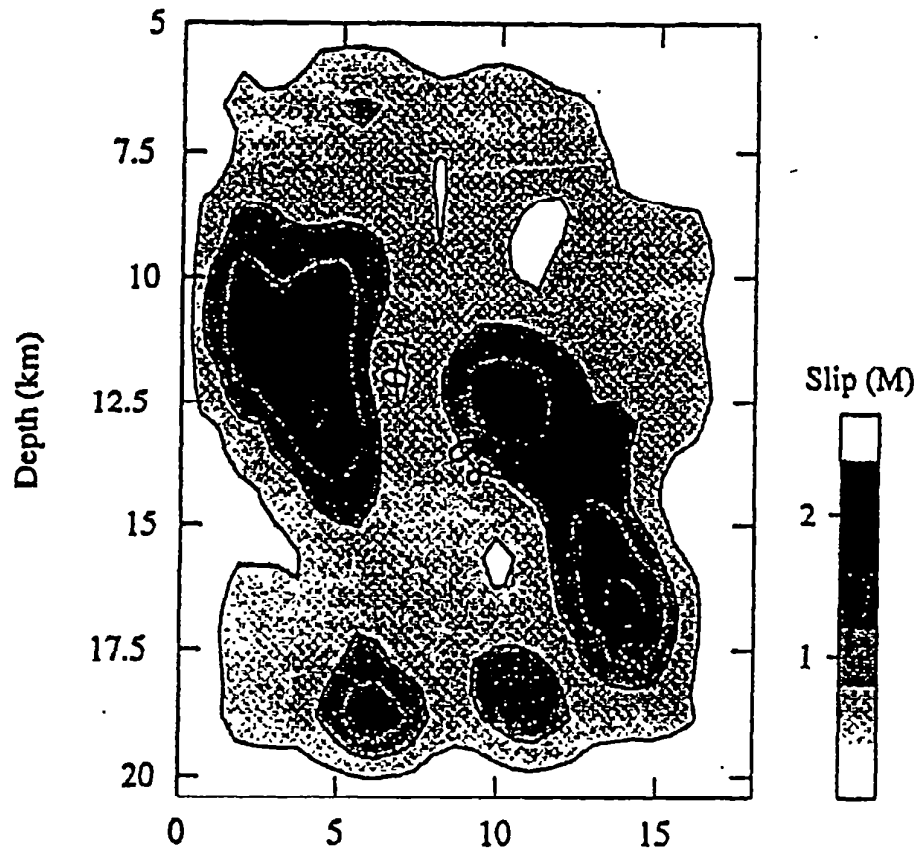
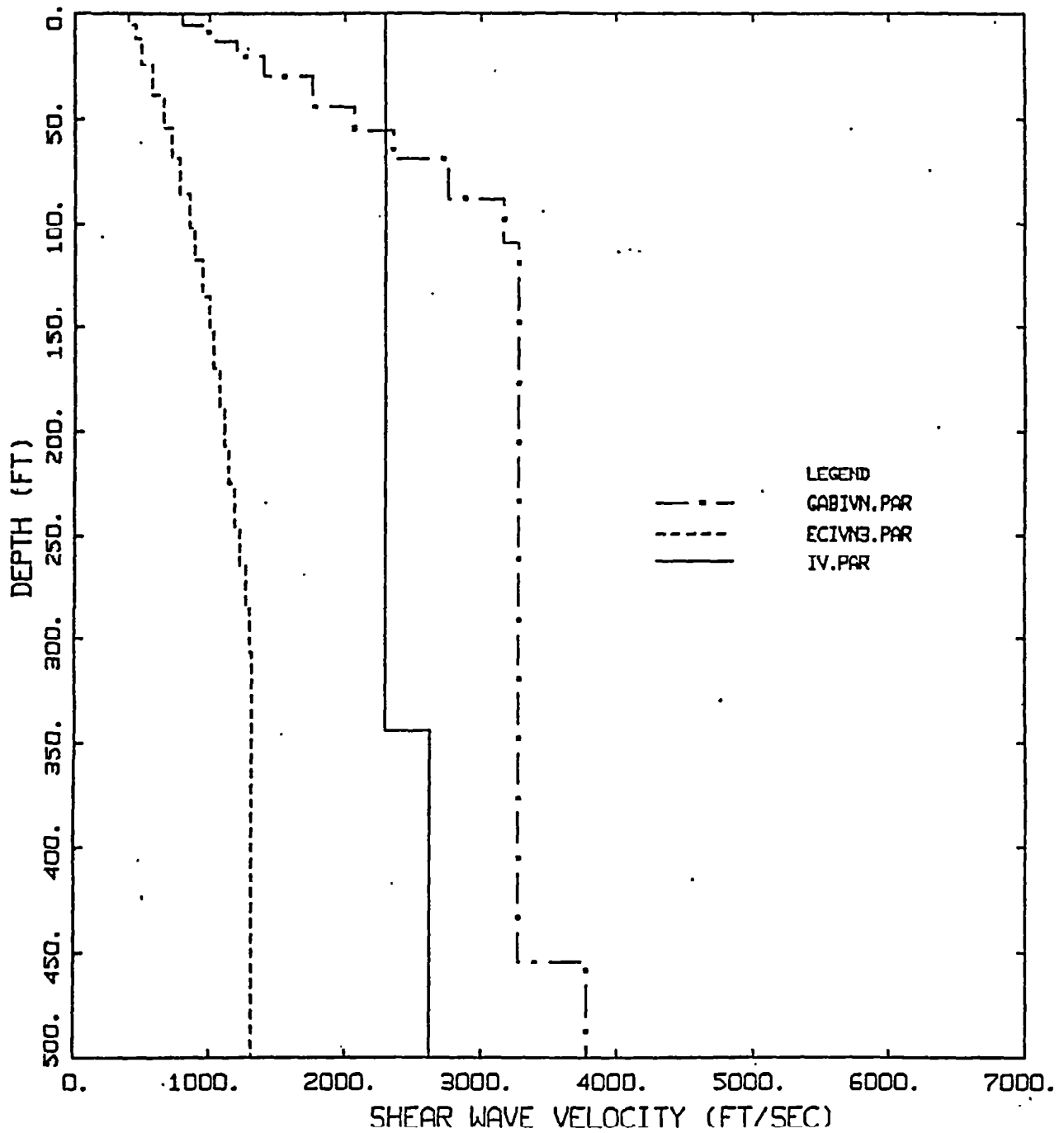
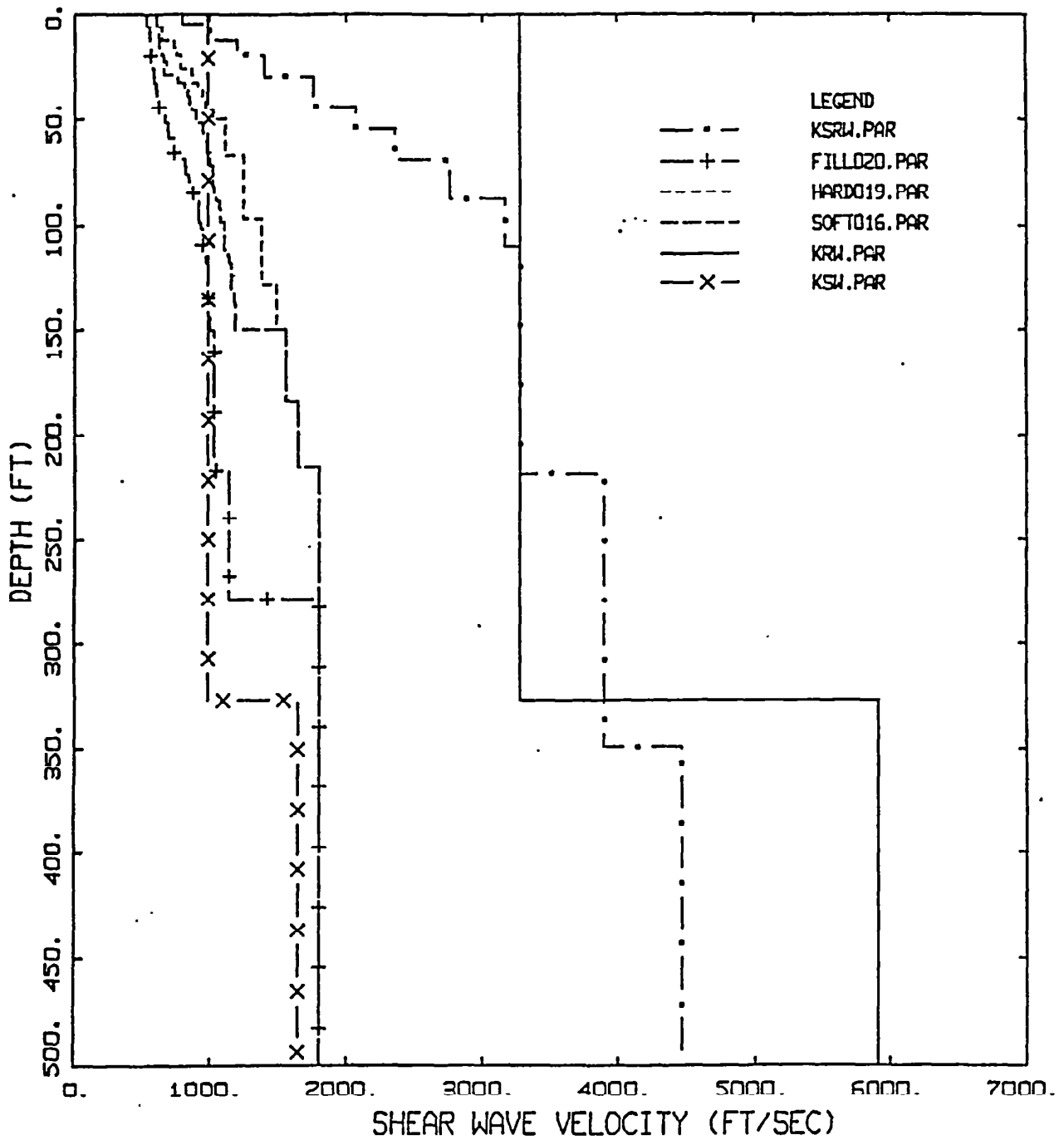


Figure 6. Slip model for the Northridge earthquake determined using rock and soil shallow shear-wave velocity profiles (Figure 4). Source, Wald et al., 1996.



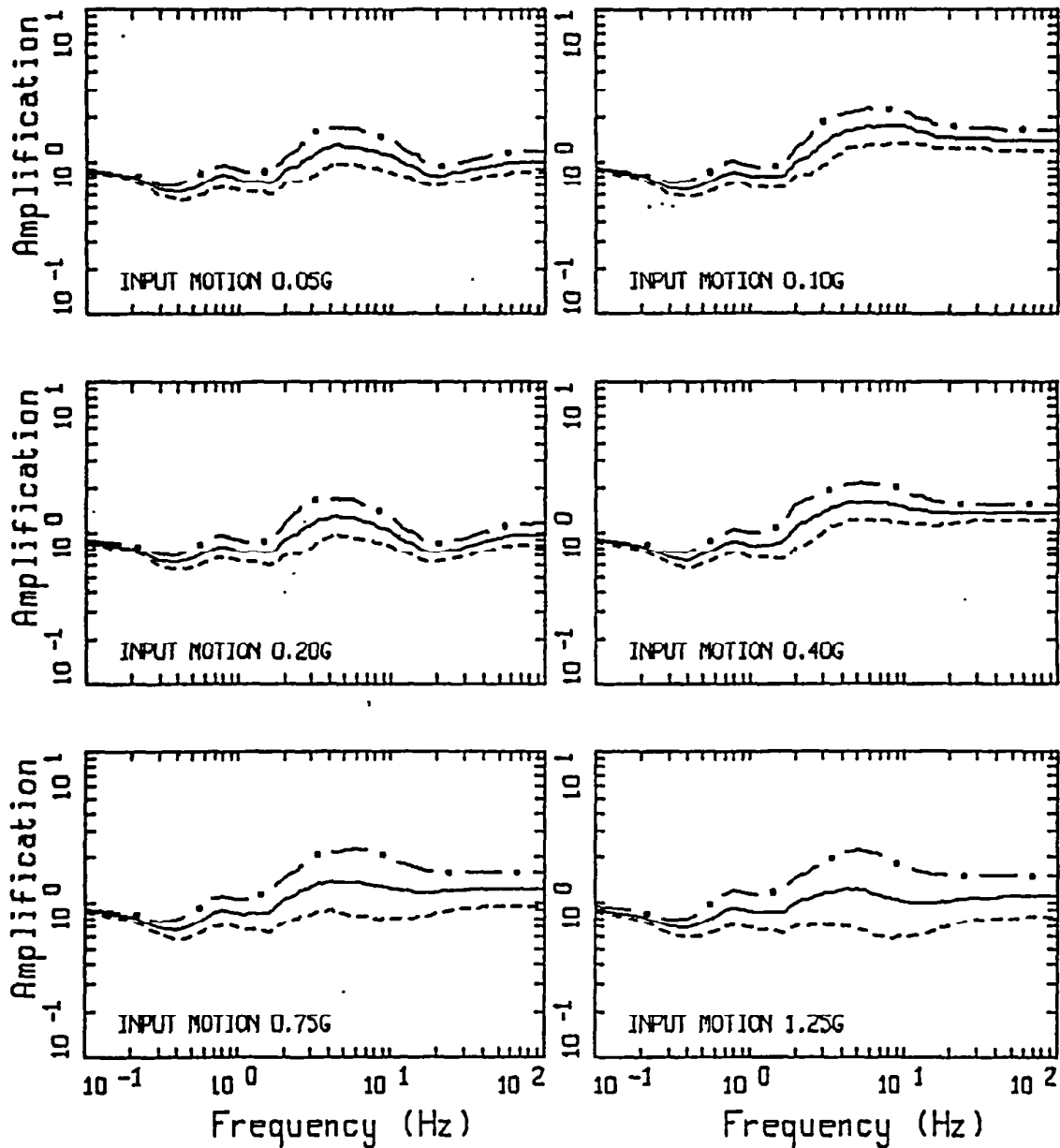
SHEAR WAVE VELOCITY PROFILE
 IMPERIAL VALLEY PROFILES

Figure 7. Shallow shear-wave velocity profiles used in modeling the Imperial Valley earthquake (rock, dash dotted; soil, dashed) and in determining the slip model (soil, solid) (Table 5).



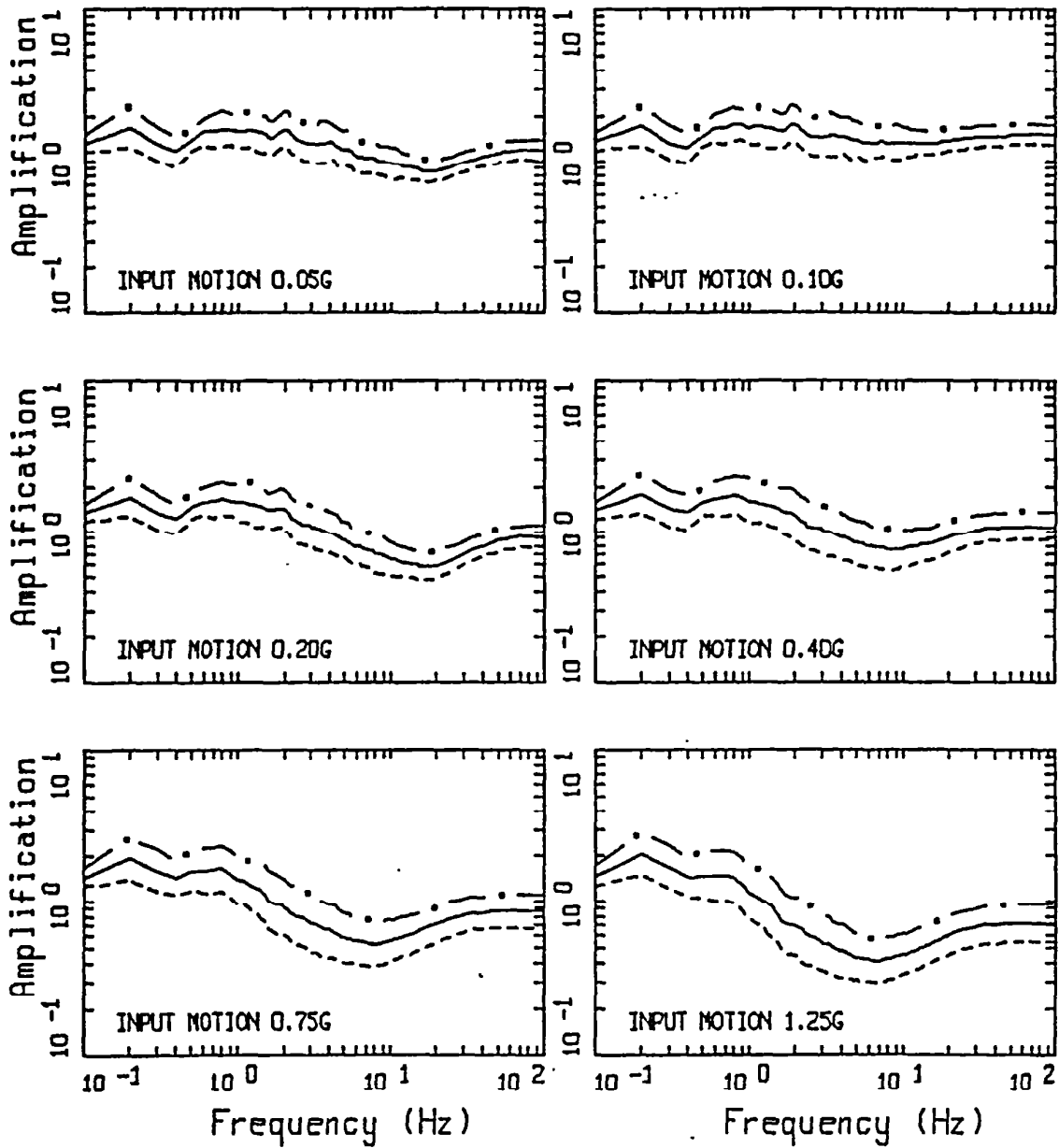
SHEAR WAVE VELOCITY PROFILE KOBE PROFILES

Figure 8. Shallow shear-wave velocity profiles used in modeling the Kobe earthquake. Rock is the dash-dotted profile and generic soil profiles were developed for alluvium (soft soil, dashed), diluvium (hard soil, short dashed) and fill (dash plus) soils. Rock (solid), and soil (dash crosses) profiles were used in developing the slip models (Table 6).



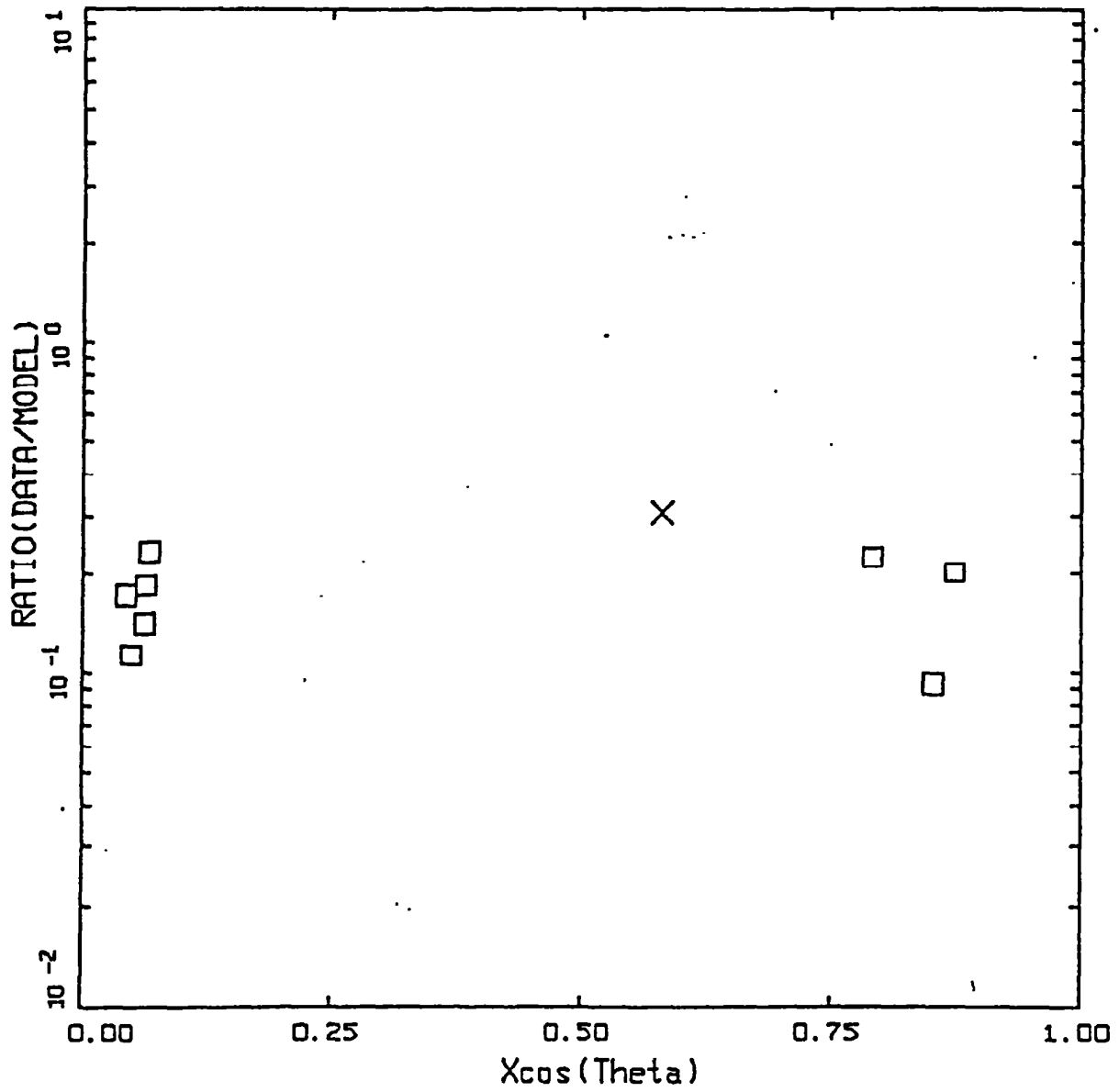
LA AMPLIFICATION (a)

Figure 9. Median and $\pm 1 \sigma$ amplification factors for 5% damped response spectra computed for generic rock (a) and generic deep soil (b) relative to the profile used in determining the site independent slip model for the Northridge earthquake.



LA AMPLIFICATION (b)
 Q_y (500 - 1500 FT) over Wald

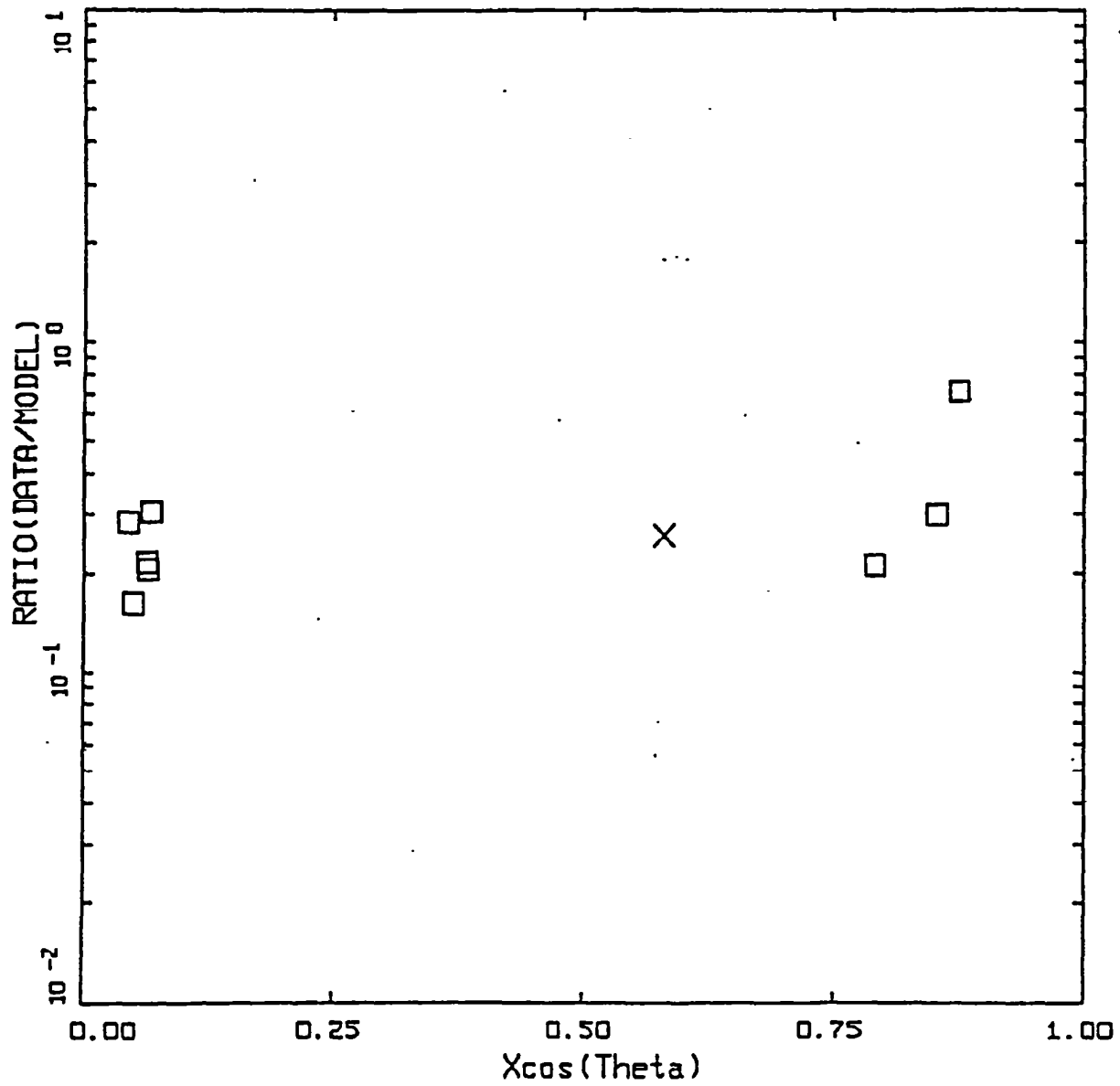
Figure 9. (Cont.)



LANDERS
 $S_a(\text{DATA})/S_a(\text{MODEL}), T=3.0 \text{ sec}$

LEGEND
 X ROCK $S_a(\text{DATA})/S_a(\text{MODEL})$
 □ SOIL $S_a(\text{DATA})/S_a(\text{MODEL})$

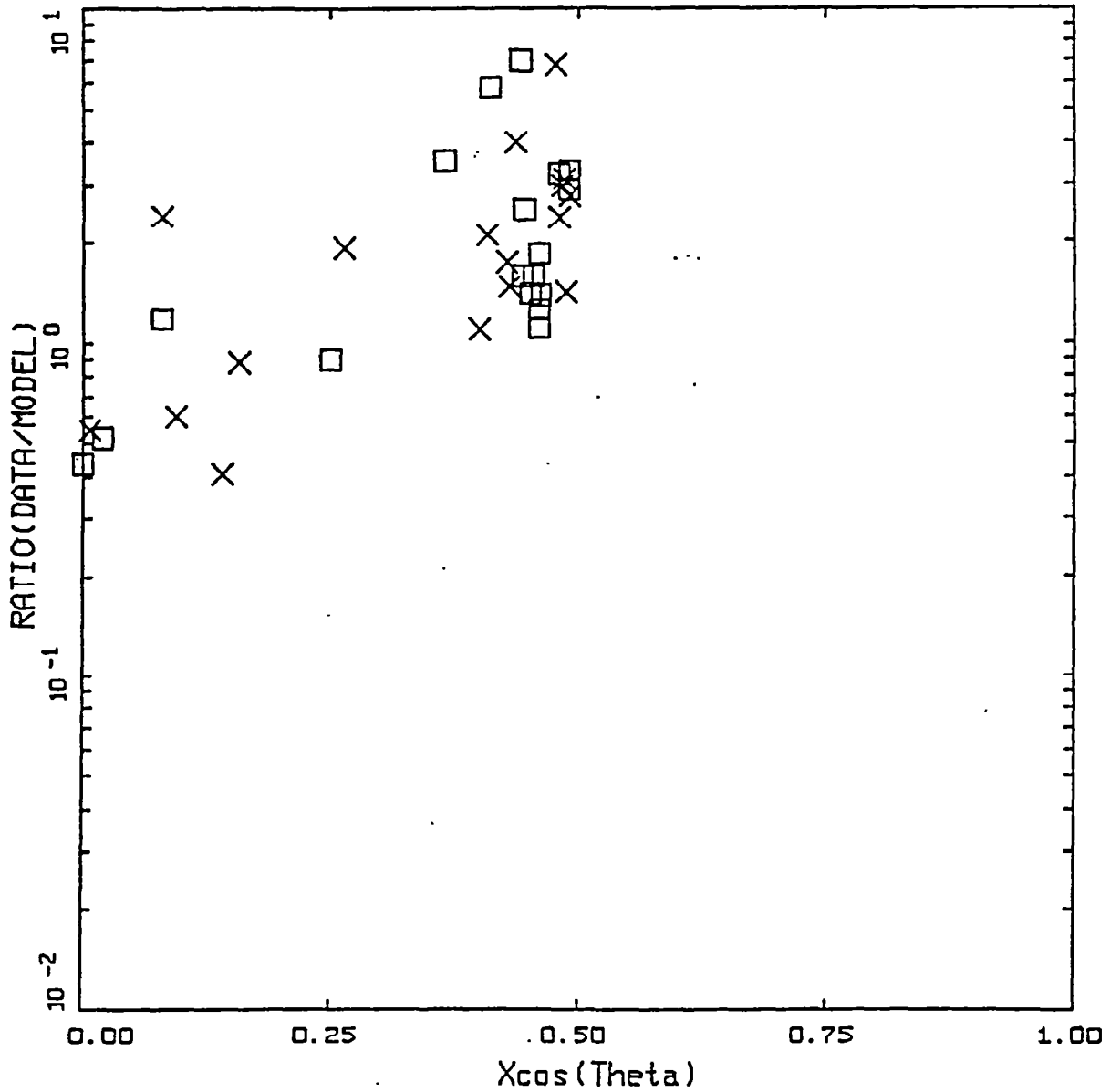
Figure 10. Ratio (data/model prediction) of 5% damped response spectra for an average horizontal component at a period of 3 sec versus directivity parameter $X \cos \theta$. Landers earthquake.



LANDERS
 $S_a(\text{DATA})/S_a(\text{MODEL}), T=5.0 \text{ sec}$

LEGEND
 X ROCK $S_a(\text{DATA})/S_a(\text{MODEL})$
 □ SOIL $S_a(\text{DATA})/S_a(\text{MODEL})$

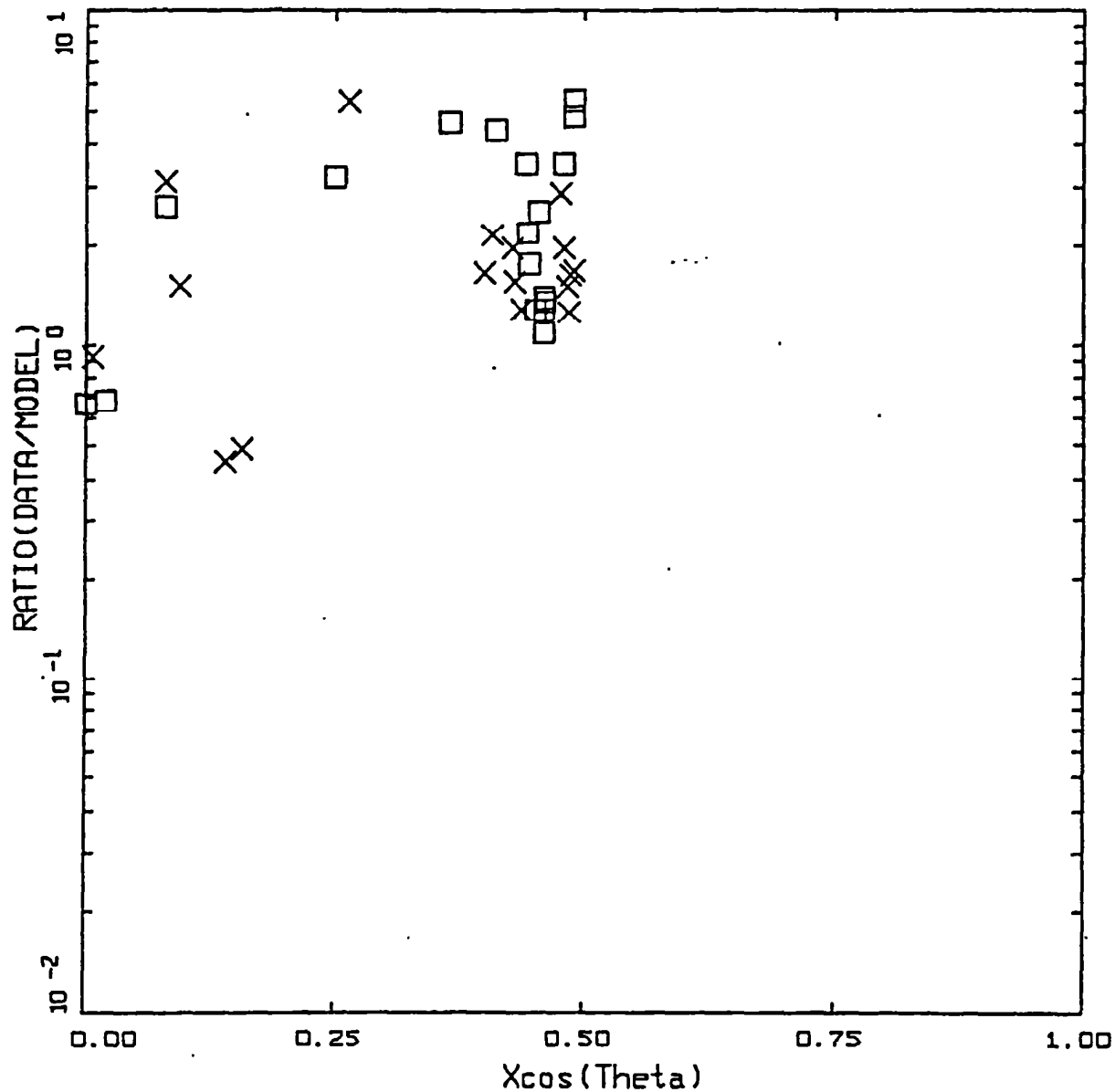
Figure 11. Ratio (data/model prediction) of 5% damped response spectra for an average horizontal component at a period of 5 sec versus directivity parameter $X \cos \theta$. Landers earthquake.



LOMA PRIETA (OH7.1)
 $S_a(\text{DATA})/S_a(\text{MODEL}), T=3.0 \text{ sec}$

LEGEND
 X ROCK $S_a(\text{DATA})/S_a(\text{MODEL})$
 □ SOIL $S_a(\text{DATA})/S_a(\text{MODEL})$

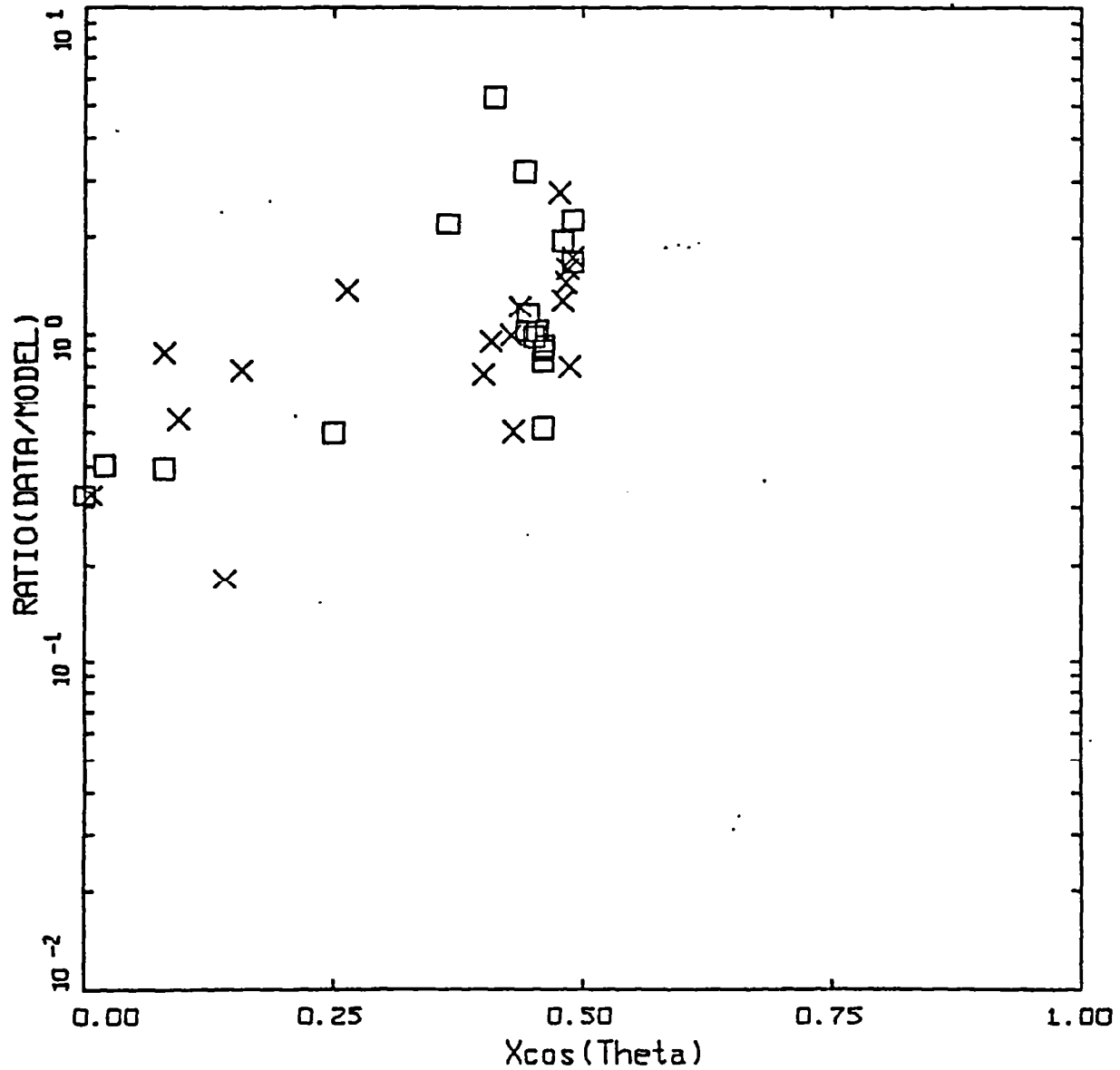
Figure 12. Ratio (data/model prediction) of 5% damped response spectra for an average horizontal component at a period of 3 sec versus directivity parameter $X \cos \theta$. Loma Prieta earthquake, rise time of 1.5 sec.



LOMA PRIETA (OH7.1)
 $S_a(\text{DATA})/S_a(\text{MODEL}), T=5.0 \text{ sec}$

LEGEND
 X ROCK $S_a(\text{DATA})/S_a(\text{MODEL})$
 □ SOIL $S_a(\text{DATA})/S_a(\text{MODEL})$

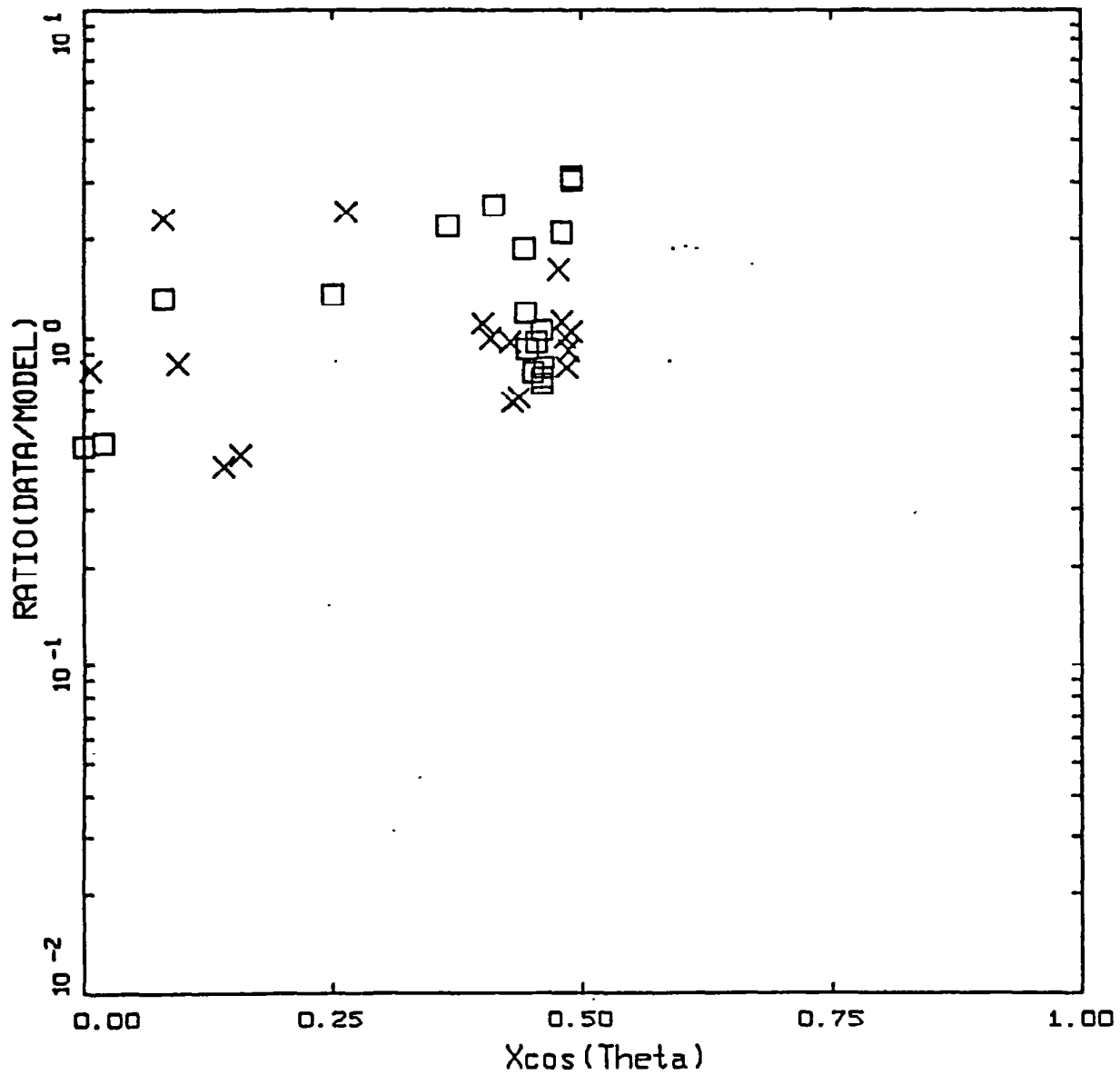
Figure 13. Ratio (data/model prediction) of 5% damped response spectra for an average horizontal component at a period of 5 sec versus directivity parameter $X \cos \theta$. Loma Prieta earthquake, rise time of 1.5 sec.



LOMA PRIETA
 $S_a(\text{DATA})/S_a(\text{MODEL}), T=3.0 \text{ sec}$

LEGEND
 X ROCK $S_a(\text{DATA})/S_a(\text{MODEL})$
 □ SOIL $S_a(\text{DATA})/S_a(\text{MODEL})$

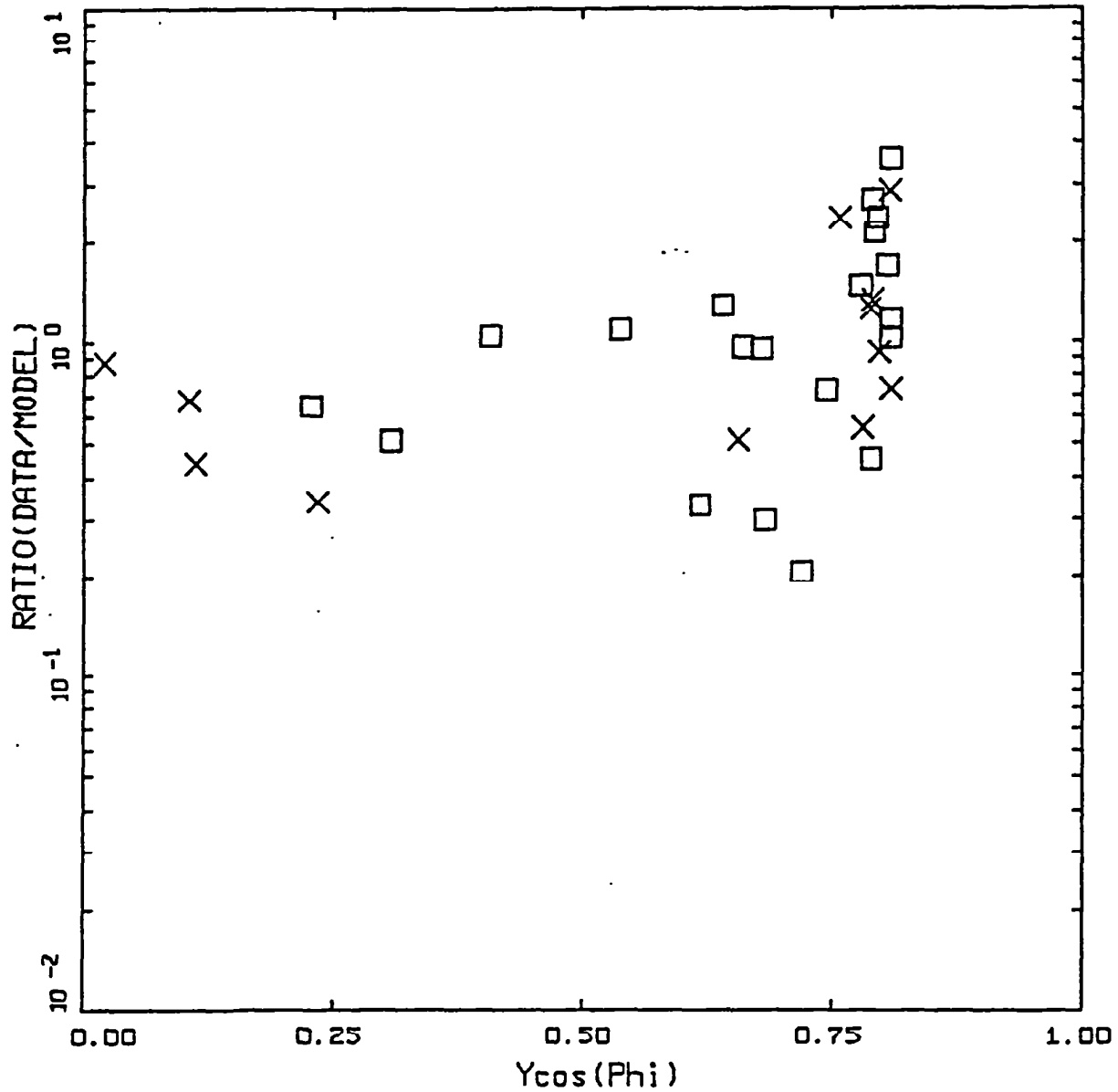
Figure 14. Ratio (data/model prediction) of 5% damped response spectra for an average horizontal component at a period of 3 sec versus directivity parameter $X \cos \theta$. Loma Prieta earthquake, rise time of 0.5 sec.



LOMA PRIETA
 $S_a(\text{DATA})/S_a(\text{MODEL}), T=5.0 \text{ sec}$

LEGEND
 X ROCK $S_a(\text{DATA})/S_a(\text{MODEL})$
 □ SOIL $S_a(\text{DATA})/S_a(\text{MODEL})$

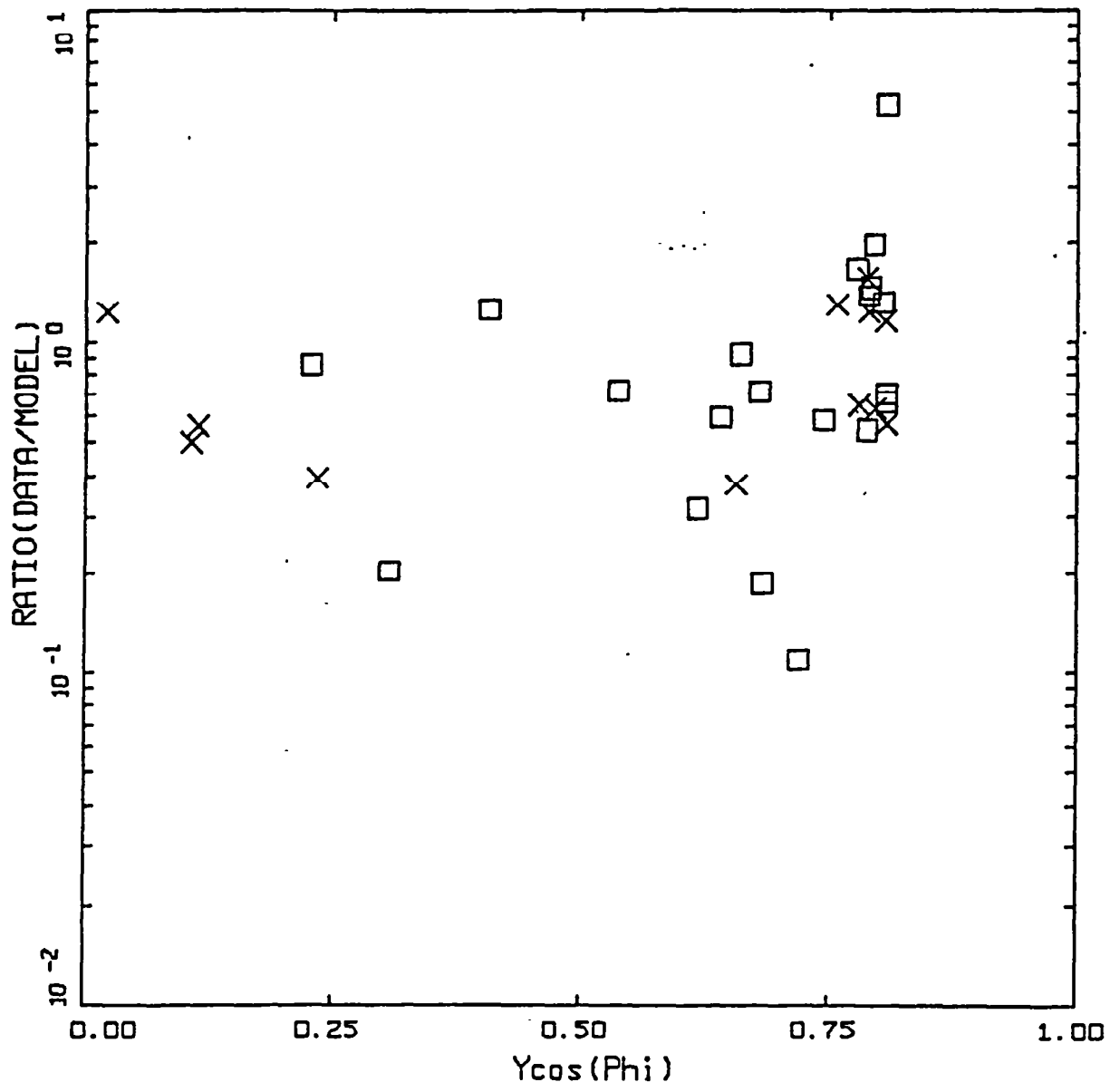
Figure 15. Ratio (data/model prediction) of 5% damped response spectra for an average horizontal component at a period of 5 sec versus directivity parameter $X \cos \theta$. Loma Prieta earthquake, rise time of 0.5 sec.

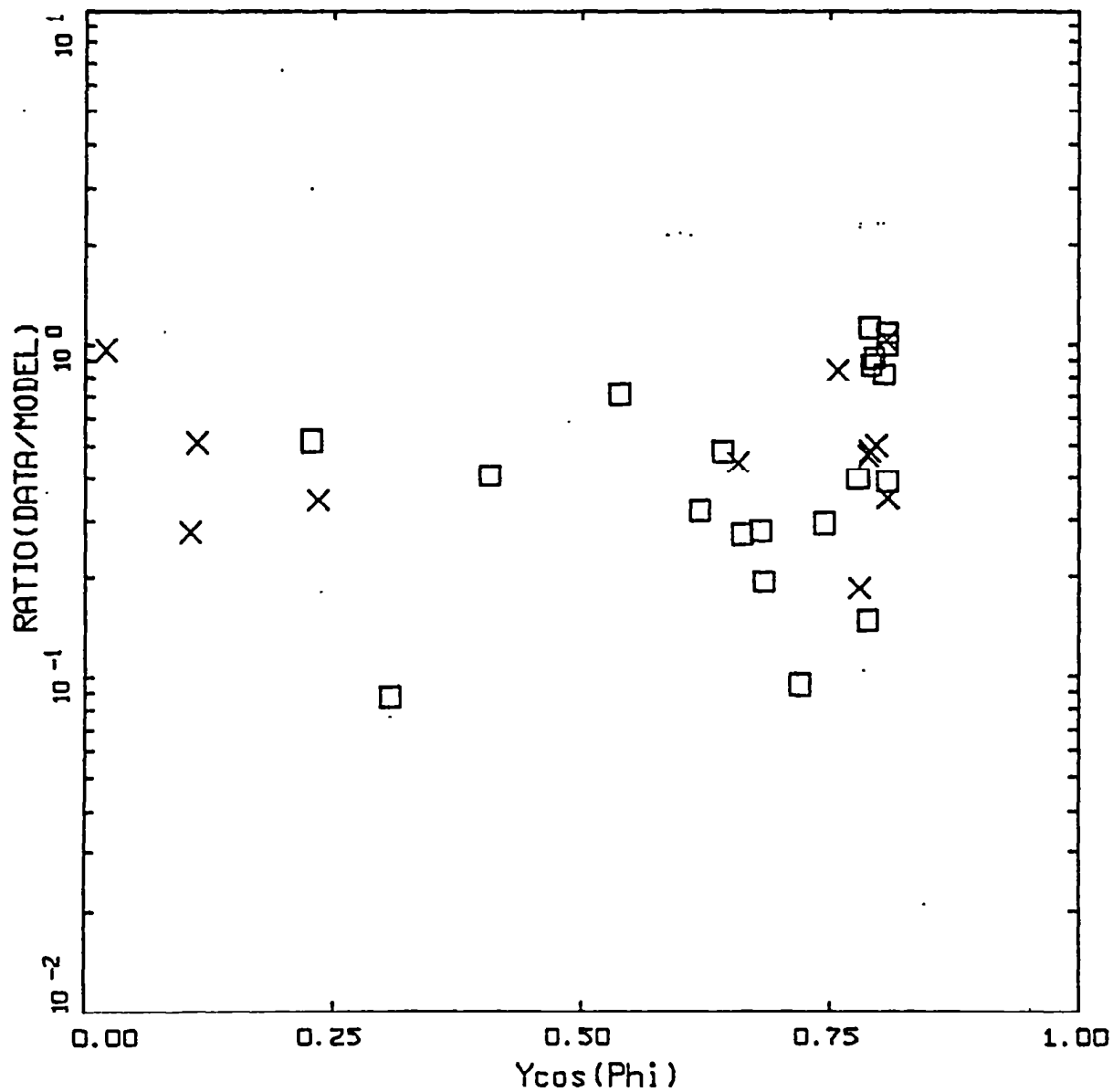


NORTHRIDGE
 $S_a(\text{DATA})/S_a(\text{MODEL}), T=3.0 \text{ sec}$

LEGEND
 X ROCK $S_a(\text{DATA})/S_a(\text{MODEL})$
 □ SOIL $S_a(\text{DATA})/S_a(\text{MODEL})$

Figure 16. Ratio (data/model prediction) of 5% damped response spectra for an average horizontal component at a period of 3 sec versus directivity parameter $Y \cos \phi$. Northridge earthquake, rise time of 1.4 sec.

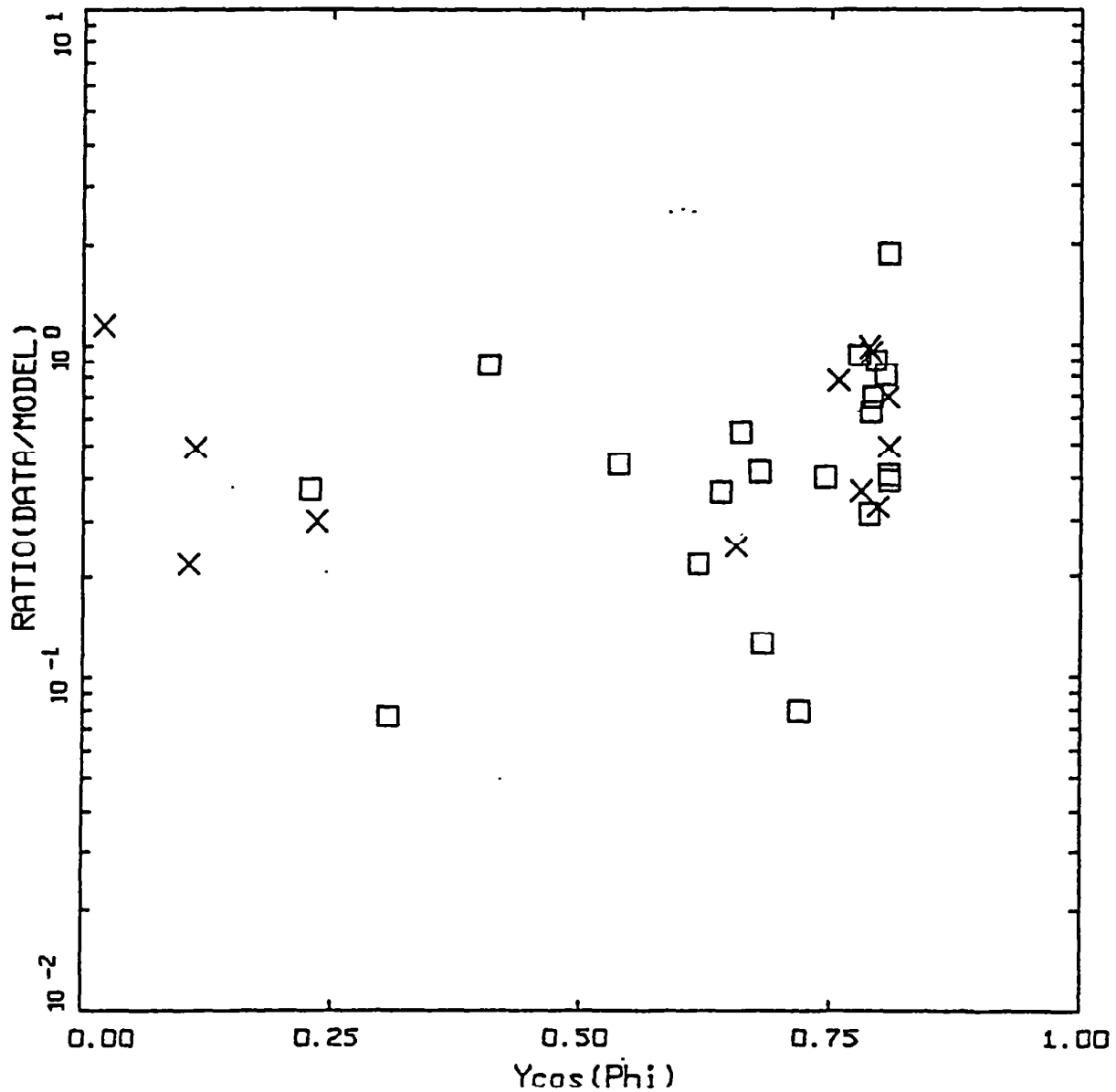




NORTHRIDGE
 $S_a(\text{DATA})/S_a(\text{MODEL}), T=3.0 \text{ sec}$

LEGEND
 X ROCK $S_a(\text{DATA})/S_a(\text{MODEL})$
 □ SOIL $S_a(\text{DATA})/S_a(\text{MODEL})$

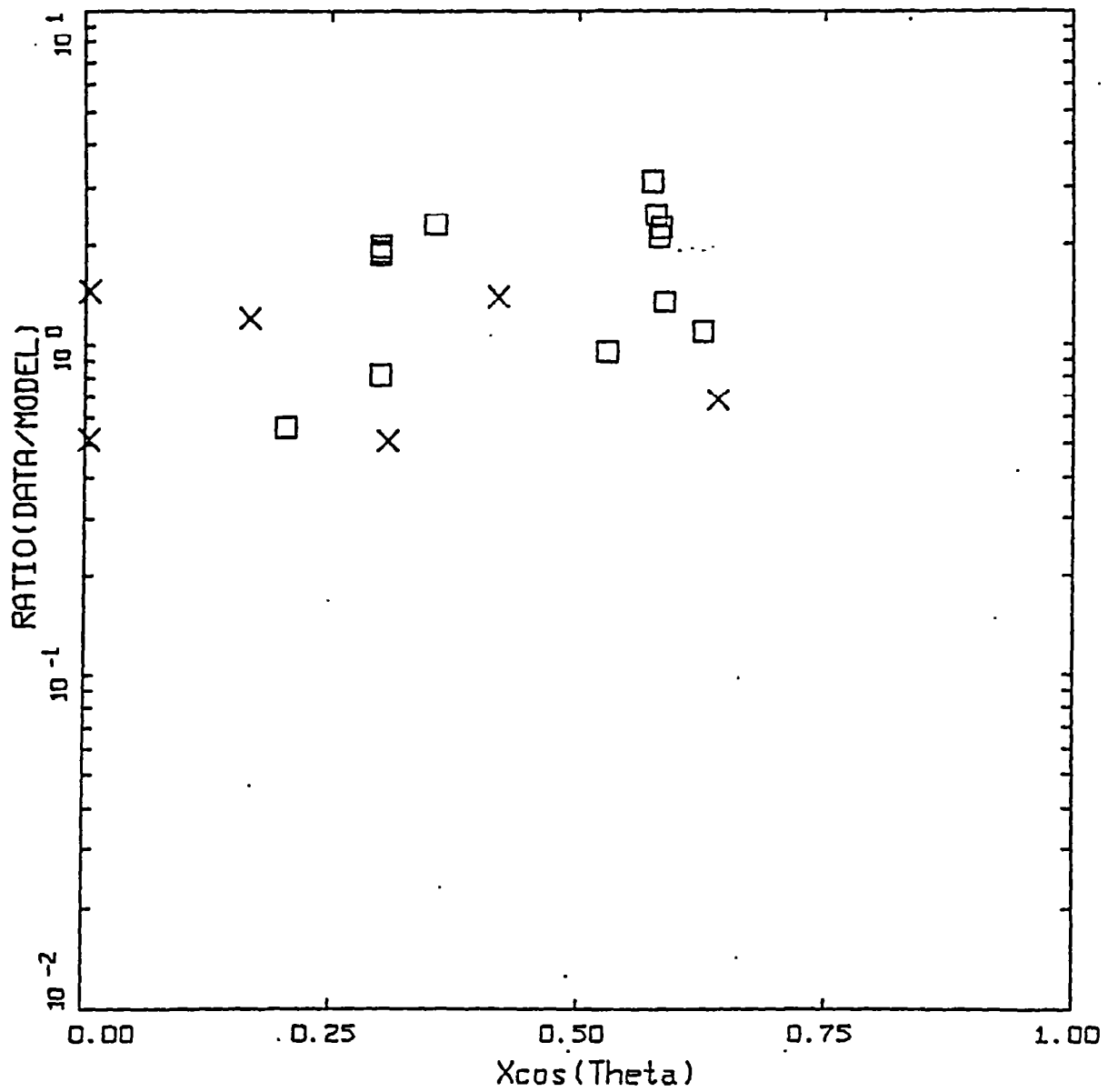
Figure 18. Ratio (data/model prediction) of 5% damped response spectra for an average horizontal component at a period of 3 sec versus directivity parameter $Y \cos \phi$. Northridge earthquake, rise time of 1.0 sec.



NORTHRIDGE
 $S_a(\text{DATA})/S_a(\text{MODEL}), T=5.0 \text{ sec}$

LEGEND
 X ROCK $S_a(\text{DATA})/S_a(\text{MODEL})$
 □ SOIL $S_a(\text{DATA})/S_a(\text{MODEL})$

Figure 19. Ratio (data/model prediction) of 5% damped response spectra for an average horizontal component at a period of 5 sec versus directivity parameter $Y \cos \phi$. Northridge earthquake, rise time of 1.0 sec.



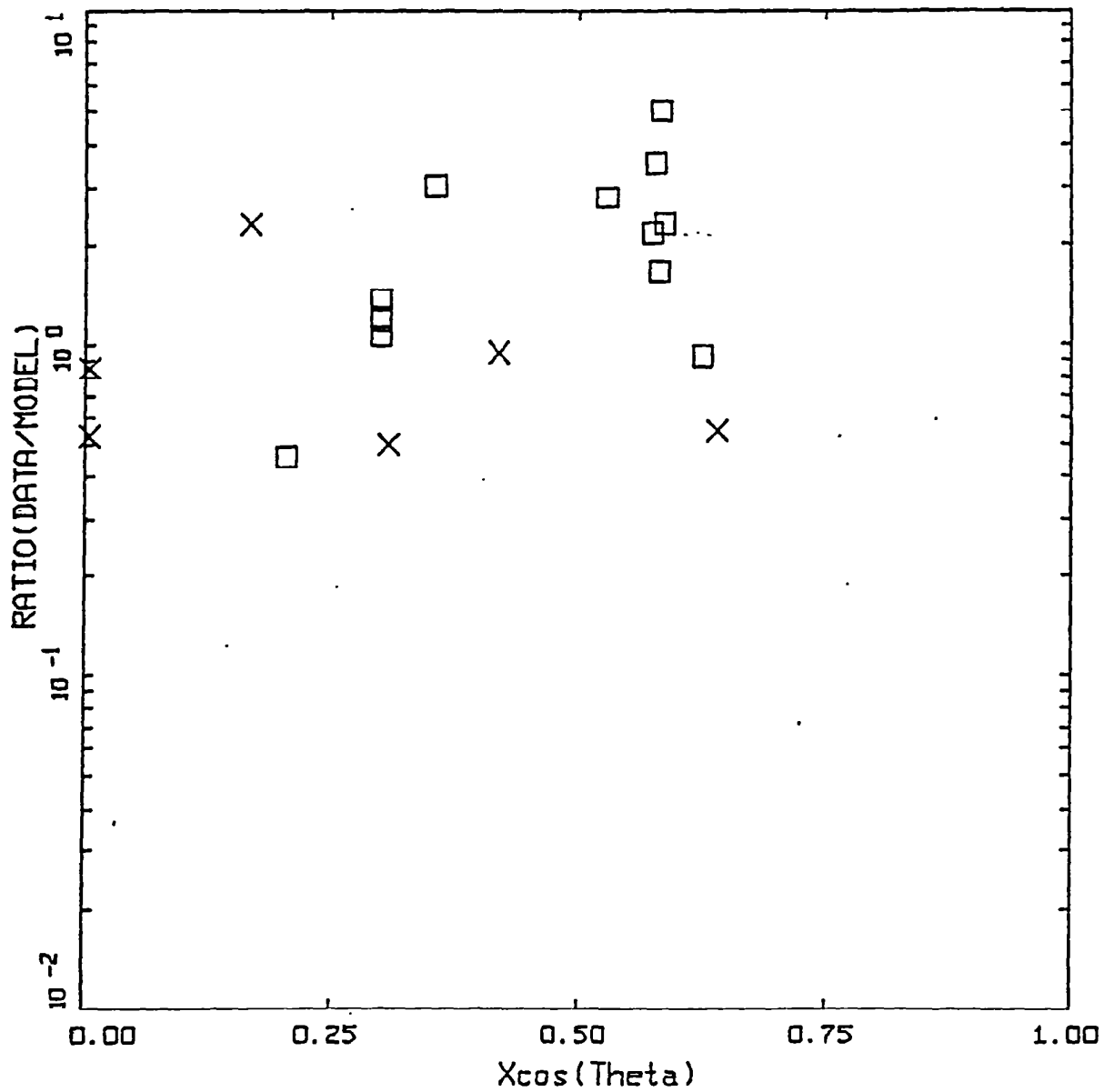
KOBE

$S_a(\text{DATA})/S_a(\text{MODEL}), T=3.0 \text{ sec}$

LEGEND

- X ROCK $S_a(\text{DATA})/S_a(\text{MODEL})$
- SOIL $S_a(\text{DATA})/S_a(\text{MODEL})$

Figure 24. Ratio (data/model prediction) of 5% damped response spectra for an average horizontal component at a period of 3 sec versus directivity parameter $X \cos \theta$. Kobe earthquake.



KOBE
 $S_a(\text{DATA})/S_a(\text{MODEL}), T=5.0 \text{ sec}$

LEGEND
 x ROCK $S_a(\text{DATA})/S_a(\text{MODEL})$
 □ SOIL $S_a(\text{DATA})/S_a(\text{MODEL})$

Figure 25. Ratio (data/model prediction) of 5% damped response spectra for an average horizontal component at a period of 5 sec versus directivity parameter $X \cos \theta$. Kobe earthquake.

APPENDIX A

STOCHASTIC GROUND MOTION MODEL DESCRIPTION

BACKGROUND

In the context of strong ground motion, the term "stochastic" can be a fearful concept to some and may be interpreted to represent a fundamentally incorrect or inappropriate model (albeit the many examples demonstrating that it works well; Boore, 1983, 1986). To allay any initial misgivings, a brief discussion seems prudent to explain the term stochastic in the stochastic ground motion model.

The stochastic point-source model may be termed a spectral model in that it fundamentally describes the Fourier amplitude spectral density at the surface of a half-space (Hanks and McGuire, 1981). The model uses a Brune (1970, 1971) omega-square description of the earthquake source Fourier amplitude spectral density. This model is easily the most widely used and qualitatively validated source description available. Seismic sources ranging from $M = -6$ (hydrofracture) to $M = 8$ have been interpreted in terms of the Brune omega-square model in dozens of papers over the last 30 years. The general conclusion is that it provides a reasonable and consistent representation of crustal sources, particularly for tectonically active regions such as plate margins. A unique phase spectrum can be associated with the Brune source amplitude spectrum to produce a complex spectrum which can be propagated using either exact or approximate (1-2- or 3-D) wave propagation algorithms to produce single or multiple component time histories. In this context the model is not stochastic, it is decidedly deterministic and as exact and rigorous as one chooses. A two-dimensional array of such point-sources may be appropriately located on a fault surface (area) and fired with suitable delays to simulate rupture propagation on an extended rupture plane (Section 2.2). As with the single point-source, any degree of rigor may be used in the wave propagation algorithm to produce multiple component or average horizontal component time histories. The result is a kinematic¹ finite-source model which has as its basis a source time history defined as a Brune pulse whose Fourier amplitude spectrum follows an omega-square model. This finite-fault model would be very similar to that used in published inversions for slip models (Chapter 4) if the 1-D propagation were treated using a reflectivity algorithm (Aki and Richards, 1980). This algorithm is a complete solution to the wave equation from static offsets (near-field terms) to an arbitrarily selected high frequency cutoff (generally 1-2 Hz).

Alternatively, to model the wave propagation more accurately, recordings of small earthquakes at the site of interest and with source locations distributed along the fault of interest may be used as empirical Green functions (Hartzell, 1978). To model the design earthquake,

¹Kinematic source model is one whose slip (displacement) is defined (imposed) while in a dynamic source model forces (stress) are defined (see Aki and Richards 1980 for a complete description).

the empirical Green functions are delayed and summed in a manner to simulate rupture propagation (Hartzell, 1978). Provided a sufficient number of small earthquakes are recorded at the site of interest, the source locations adequately cover the expected rupture surface, and sufficient low frequency energy is present in the Green functions, this would be the most appropriate procedure to use if nonlinear site response is not an issue. With this approach the wave propagation is, in principle, exactly represented from each Green function source to the site. However, nonlinear site response is not treated unless Green function motions are recorded at a nearby rock outcrop with dynamic material properties similar to the rock underlying the soils at the site or recordings are made at depth within the site soil column. These motions may then be used as input to either total or effective stress site response codes to model nonlinear effects. Important issues associated with this approach include the availability of an appropriate nearby (1 to 2 km) rock outcrop and, for the downhole recordings, the necessity to remove all downgoing energy from the at-depth soil recordings. The downgoing energy must be removed from the downhole Green functions (recordings) prior to generating the control motions (summing) as only the upgoing wavefields are used as input to the nonlinear site response analyses. Removal of the downgoing energy from each recording requires multiple site response analyses which introduce uncertainty into the Green functions due to uncertainty in dynamic material properties and the numerical site response model used to separate the upgoing and downgoing wavefields.

To alleviate these difficulties one can use recordings well distributed in azimuth at close distances to a small earthquake and correct the recordings back to the source by removing wave propagation effects using a simple approximation (say $1/R$ plus a constant for crustal amplification and radiation pattern), to obtain an empirical source function. This source function can be used to replace the Brune pulse to introduce some natural (although source, path, and site specific) variation into the dislocation time history. If this is coupled to an approximate wave propagation algorithm (asymptotic ray theory) which includes the direct rays and those which have undergone a single reflection, the result is the empirical source function method (EPRI, 1993). Combining the reflectivity propagation (which is generally limited to frequencies ≤ 1 -2 Hz due to computational demands) with the empirical source function approach (appropriate for frequencies ≥ 1 Hz; EPRI, 1993) results in a broad band simulation procedure which is strictly deterministic at low frequencies (where an analytical source function is used) and incorporates some natural variation at high frequencies through the use of an empirical source function (Sommerville et al., 1995).

All of these techniques are fundamentally similar, well founded in seismic source and wave propagation physics, and importantly, they are all approximate. Simply put, all models are wrong (approximate) and the single essential element in selecting a model is to incorporate the appropriate degree of rigor, commensurate with uncertainties and variabilities in crustal structure and site effects, through extensive validation exercises. It is generally felt that more complicated models produce more accurate results, however, the implications of more sophisticated models with the increased number of parameters which must be specified is often overlooked. This is not too serious a consequence in modeling past earthquakes since a reasonable range in parameter space can be explored to give the "best" results. However for future predictions, this increased rigor may carry undesirable baggage in increased parametric variability (Roble et al., 1996). The effects of lack of knowledge (epistemic uncertainty; EPRI,

1993) regarding parameter values for future occurrences results in uncertainty or variability in ground motion predictions. It may easily be the case that a very simple model, such as the point-source model can have comparable, or even smaller, total variability (modeling plus parametric) than a much more rigorous model with an increased number of parameters (EPRI, 1993). What is desired in a model is sufficient sophistication such that it captures the dominant and stable features of source, distance, and site dependencies observed in strong ground motions. It is these considerations which led to the development of the stochastic point- and finite-source models and, in part, leads to the stochastic element of the models.

The stochastic nature of the point- and finite-source RVT models is simply the assumption made about the character of ground motion time histories that permits stable estimates of peak parameters (e.g. acceleration, velocity, strain, stress, oscillator response) to be made without computing detailed time histories (Hanks and McGuire, 1981; Boore, 1983). This process uses random vibration theory to relate a time domain peak value to the time history root-mean-square (RMS) value (Boore, 1983). The assumption of the character of the time history for this process to strictly apply is that it be normally distributed random noise and stationary (its statistics do not change with time) over its duration. A visual examination of any time history quickly reveals that this is clearly not the case: time histories (acceleration, velocity, stress, strain, oscillator) start, build up, and then diminish with time. However poor the assumption of stationary Gaussian noise may appear, the net result is that the assumption is weak enough to permit the approach to work surprisingly well, as numerous comparisons with recorded motions and both qualitative and quantitative validations have shown (Hanks and McGuire, 1981; Boore, 1983, 1986; McGuire et al., 1984; Boore and Atkinson, 1987; Silva and Lee, 1987; Toro and McGuire, 1987; Silva et al., 1990; EPRI, 1993; Schneider et al., 1993; Silva and Darragh, 1995; Silva et al., 1997). Corrections to RVT are available to accommodate different distributions as well as non-stationarity and are usually applied to the estimation of peak oscillator response in the calculated response spectra (Boore and Joyner, 1984; Toro, 1985).

Point-source Model

The conventional stochastic ground motion model uses an ω -square source model (Brune, 1970, 1971) with a single corner frequency and a constant stress drop (Boore, 1983; Atkinson, 1984). Random vibration theory is used to relate RMS (root-mean-square) values to peak values of acceleration (Boore, 1983), and oscillator response (Boore and Joyner, 1984; Toro, 1985; Silva and Lee, 1987) computed from the power spectra to expected peak time domain values (Boore, 1983).

The shape of the acceleration spectral density, $a(f)$, is given by

$$a(f) = C \frac{f^2}{1 + \left(\frac{f}{f_0}\right)^2} \frac{M_0}{R} P(f) A(f) e^{-\frac{\pi f R}{\beta_0 Q(f)}} \quad (\text{A-1})$$

where

$$C = \left(\frac{1}{\rho_0 \beta_0^3}\right) \cdot (2) \cdot (0.55) \cdot \left(\frac{1}{\sqrt{2}}\right) \cdot \pi.$$

- M_0 = seismic moment,
- R = hypocentral distance,
- β_0 = shear-wave velocity at the source,
- ρ_0 = density at the source
- $Q(f)$ = frequency dependent quality factor (crustal damping),
- $A(f)$ = crustal amplification,
- $P(f)$ = high-frequency truncation filter,
- f_0 = source corner frequency.

C is a constant which contains source region density (ρ_0) and shear-wave velocity terms and accounts for the free-surface effect (factor of 2), the source radiation pattern averaged over a sphere (0.55) (Boore, 1986), and the partition of energy into two horizontal components ($1/\sqrt{2}$).

Source scaling is provided by specifying two independent parameters, the seismic moment (M_0) and the high-frequency stress parameter or stress drop ($\Delta\sigma$). The seismic moment is related to magnitude through the definition of moment magnitude M by the relation

$$\log M_0 = 1.5 M + 16.05 \quad (\text{Hanks and Kanamori, 1979}) \quad (\text{C-2}).$$

The stress drop ($\Delta\sigma$) relates the corner frequency f_0 to M_0 through the relation

$$f_0 = \beta_0 (\Delta\sigma/8.44 M_0)^{1/3} \quad (\text{Brune; 1970, 1971}) \quad (\text{C-3}).$$

The stress drop is sometimes referred to as the high frequency stress parameter (Boore, 1983) (or simply the stress parameter) since it directly scales the Fourier amplitude spectrum for frequencies above the corner frequency (Silva, 1991; Silva and Darragh 1995). High (> 1 Hz) frequency model predictions are then very sensitive to this parameter (Silva, 1991; EPRI, 1993) and the interpretation of it being a stress drop or simply a scaling parameter depends upon how well real earthquake sources (on average) obey the omega-square scaling (Equation A-3) and how well they are fit by the single-corner-frequency model. If earthquakes truly have single-corner-frequency omega-square sources, the stress drop in Equation A-3 is a physical parameter and its values have a physical interpretation of the forces (stresses) accelerating the relative slip across the rupture surface. High stress drop sources are due to a smaller source (fault) area (for the same M) than low stress drop sources (Brune, 1970). Otherwise, it simply a high frequency scaling or fitting parameter.

The spectral shape of the single-corner-frequency ω -square source model is then described by the two free parameters M_0 and $\Delta\sigma$. The corner frequency increases with the shear-wave velocity and with increasing stress drop, both of which may be region dependent.

The crustal amplification accounts for the increase in wave amplitude as seismic energy travels through lower-velocity crustal materials from the source to the surface. The amplification depends on average crustal and near surface shear-wave velocity and density (Boore, 1986).

The P(f) filter is used in an attempt to model the observation that acceleration spectral density appears to fall off rapidly beyond some region- or site-dependent maximum frequency (Hanks, 1982; Silva and Darragh, 1995). This observed phenomenon truncates the high frequency portion of the spectrum and is responsible for the band-limited nature of the stochastic model. The band limits are the source corner frequency at low frequency and the high frequency spectral attenuation. This spectral fall-off at high frequency has been attributed to near-site attenuation (Hanks, 1982; Anderson and Hough, 1984) or to source processes (Papageorgiou and Aki, 1983) or perhaps to both effects. In the Anderson and Hough (1984) attenuation model, adopted here, the form of the P(f) filter is taken as

$$P(f, r) = e^{-\pi\kappa(r)f} \quad (\text{A-4}).$$

Kappa (r) ($\kappa(r)$ in Equation C-4) is a site and distance dependent parameter that represents the effect of intrinsic attenuation upon the wavefield as it propagates through the crust from source to receiver. Kappa (r) depends on epicentral distance (r) and on both the shear-wave velocity (β) and quality factor (Q_s) averaged over a depth of H beneath the site (Hough et al., 1988). At zero epicentral distance kappa (κ) is given by

$$\kappa(0) = \frac{H}{\bar{\beta} \bar{Q}_s} \quad (\text{A-5}),$$

and is referred to as κ .

The bar in Equation C-5 represents an average of these quantities over a depth H. The value of kappa at zero epicentral distance is attributed to attenuation in the very shallow crust directly below the site (Hough and Anderson, 1988; Silva and Darragh, 1995). The intrinsic attenuation along this part of the path is not thought to be frequency dependent and is modeled as a frequency independent, but site and crustal region dependent, constant value of kappa (Hough et al., 1988; Rovelli et al., 1988). This zero epicentral distance kappa is the model implemented in this study.

The crustal path attenuation from the source to just below the site is modeled with the frequency- dependent quality factor Q(f). Thus the distance component of the original $\kappa(r)$ (Equation A-4) is accommodated by Q(f) and R in the last term of Equation A-1:

$$\kappa(r) = \frac{H}{\beta Q_s} + \frac{R}{\beta_0 Q(f)} \quad (\text{A-6}).$$

The Fourier amplitude spectrum, $a(f)$, given by Equation C-1 represents the stochastic ground motion model employing a Brune source spectrum that is characterized by a single corner frequency. It is a point source and models direct shear-waves in a homogeneous half-space (with effects of a velocity gradient captured by the $A(f)$ filter, Equation A-1). For horizontal motions, vertically propagating shear-waves are assumed. Validations using incident inclined SH-waves accompanied with raytracing to find appropriate incidence angles leaving the source showed little reduction in uncertainty compared to results using vertically propagating shear-waves. For vertical motions, P/SV propagators are used coupled with raytracing to model incident inclined plane waves (EPRI, 1993). This approach has been validated with recordings from the 1989 M 6.9 Loma Prieta earthquake (EPRI, 1993).

Equation C-1 represents an elegant ground motion model that accommodates source and wave propagation physics as well as propagation path and site effects with an attractive simplicity. The model is appropriate for an engineering characterization of ground motion since it captures the general features of strong ground motion in terms of peak acceleration and spectral composition with a minimum of free parameters (Boore, 1983; McGuire et al., 1984; Boore, 1986; Silva and Green, 1988; Silva et al., 1988; Schneider et al., 1993; Silva and Darragh, 1995). An additional important aspect of the stochastic model employing a simple source description is that the region-dependent parameters may be evaluated by observations of small local or regional earthquakes. Region-specific seismic hazard evaluations can then be made for areas with sparse strong motion data with relatively simple spectral analyses of weak motion (Silva, 1992).

In order to compute peak time-domain values, i.e. peak acceleration and oscillator response, RVT is used to relate RMS computations to peak value estimates. Boore (1983) and Boore and Joyner (1984) present an excellent development of the RVT methodology as applied to the stochastic ground motion model. The procedure involves computing the RMS value by integrating the power spectrum from zero frequency to the Nyquist frequency and applying Parsevall's relation. Extreme value theory is then used to estimate the expected ratio of the peak value to the RMS value of a specified duration of the stochastic time history. The duration is taken as the inverse of the source corner frequency (Boore, 1983).

Factors that affect strong ground motions such as surface topography, finite and propagating seismic sources, laterally varying near-surface velocity and Q gradients, and random inhomogeneities along the propagation path are not included in the model. While some or all of these factors are generally present in any observation of ground motion and may exert controlling influences in some cases, the simple stochastic point-source model appears to be robust in predicting median or average properties of ground motion (Boore 1983, 1986; Schneider et al., 1993; Silva and Stark, 1993). For this reason it represents a powerful predictive and interpretative tool for engineering characterization of strong ground motion.

Finite-source Model Ground Motion Model

In the near-source region of large earthquakes, aspects of a finite-source including rupture propagation, directivity, and source-receiver geometry can be significant and may be incorporated into strong ground motion predictions. To accommodate these effects, a methodology that combines the aspects of finite-earthquake-source modeling techniques (Hartzell, 1978; Irikura 1983) with the stochastic point-source ground motion model has been developed to produce response spectra as well as time histories appropriate for engineering design (Silva et al., 1990; Silva and Stark, 1993; Schneider et al., 1993). The approach is very similar to the empirical Green function methodology introduced by Hartzell (1978) and Irikura (1983). In this case however, the stochastic point-source is substituted for the empirical Green function and peak amplitudes; PGA, PGV, and response spectra (when time histories are not produced) are estimated using random process theory.

Use of the stochastic point-source as a Green function is motivated by its demonstrated success in modeling ground motions in general and strong ground motions in particular (Boore, 1983, 1986; Silva and Stark, 1993; Schneider et al., 1993; Silva and Darragh, 1995) and the desire to have a model that is truly site- and region-specific. The model can accommodate a region specific $Q(f)$, Green function sources of arbitrary moment or stress drop, and site specific κ values. The necessity for having available regional and site specific recordings or modifying possibly inappropriate empirical Green functions is eliminated.

For the finite-source characterization, a rectangular fault is discretized into NS subfaults of moment M_0^s . The empirical relationship

$$\log (A) = M - 4.0, \quad A \text{ in km}^2 \quad (\text{A-7}).$$

is used to assign areas to both the target earthquake (if its rupture surface is not fixed) as well as to the subfaults. This relation results from regressing log area on M using the data of Wells and Coppersmith (1994). In the regression, the coefficient on M is set to unity which implies a constant static stress drop of about 30 bars (Equation A-9). This is consistent with the general observation of a constant static stress drop for earthquakes based on aftershock locations (Wells and Coppersmith 1994). The static stress drop, defined by Equation A-10, is related to the average slip over the rupture surface as well as rupture area. It is theoretically identical to the stress drop in Equation A-3 which defines the omega-square source corner frequency assuming the rupture surface is a circular crack model (Brune, 1970; 1971). The stress drop determined by the source corner frequency (or source duration) is usually estimated through the Fourier amplitude spectral density while the static stress drop uses the moment magnitude and an estimate of the rupture area. The two estimates for the same earthquake seldom yield the same values with the static generally being the smaller. In a recent study (Silva et al., 1997), the average stress drop based on Fourier amplitude spectra determined from an empirical attenuation relation (Abrahamson and Silva, 1997) is about 70 bars while the average static stress drop for the crustal earthquakes studied by Wells and Coppersmith (1994) is about 30 bars. These results reflect a general factor of about 2 on average between the two values. These large differences

may simply be the result of using an inappropriate estimate of rupture area as the zone of actual slip is difficult to determine unambiguously. In general however, even for individual earthquakes, the two stress drops scale similarly with high static stress drops (> 30 bars) resulting in large high frequency (> 1 Hz for $M \geq 5$) ground motions which translates to high corner frequencies (Equation A-3).

The subevent magnitude M_s is generally taken in the range of 5.0-6.5 depending upon the size of the target event. M_s 5.0 is used for crustal earthquakes with M in the range of 5.5 to 8.0 and M_s 6.4 is used for large subduction earthquakes with $M > 7.5$. The value of NS is determined as the ratio of the target event area to the subfault area. To constrain the proper moment, the total number of events summed (N) is given by the ratio of the target event moment to the subevent moment. The subevent and target event rise times (duration of slip at a point) are determined by the equation

$$\log \tau = 0.33 \log M_0 - 8.54 \quad (\text{A-8})$$

which results from a fit to the rise times used in the finite-fault modeling exercises, (Silva et al., 1997). Slip on each subfault is assumed to continue for a time τ . The ratio of target-to-subevent rise times is given by

$$\frac{\tau}{\tau^*} = 10^{0.5(M - M^*)} \quad (\text{A-9})$$

and determines the number of subevents to sum in each subfault. This approach is generally referred to as the constant-rise-time model and results in variable slip velocity for nonuniform slip distributions. Alternatively, one can assume a constant slip velocity resulting in a variable-rise-time model for heterogenous slip distributions.

Recent modeling of the Landers (Wald and Heaton, 1994), Kobe (Wald, 1996) and Northridge (Hartzell et al. 1996) earthquakes suggests that a mixture of both constant rise time and constant slip velocity may be present. Longer rise times seem to be associated with areas of larger slip with the ratio of slip-to-rise time (slip velocity) being depth dependent. Lower slip velocities (longer rise times) are associated with shallow slip resulting in relatively less short period seismic radiation. This result may explain the general observation that shallow slip is largely aseismic. The significant contributions to strong ground motions appear to originate at depths exceeding about 4 km (Campbell, 1993; Boore et al., 1994) as the fictitious depth term in empirical attenuation relation (Abrahamson and Silva, 1997; Boore et al., 1997). Finite-fault models generally predict unrealistically large strong ground motions for large shallow (near surface) slip using rise times or slip velocities associated with deeper (> 4 km) zones of slip. This is an important and unresolved issue in finite-fault modeling and the general approach is constrain the slip to relatively small values in the top 2 to 4 km. A more thorough analysis is necessary, ideally using several well validated models, before this issue can be satisfactorily

resolved.

To introduce heterogeneity of the earthquake source process into the stochastic finite-fault model, the location of the sub-events within each subfault (Hartzell, 1978) are randomized as well as the subevent rise time. The stress drop of the stochastic point-source Green function is taken as 30 bars, consistent with the static value based on the M 5.0 subevent area using the equation

$$\Delta\sigma = \frac{7}{16} \left(\frac{M_s}{R_s^3} \right) \quad (\text{Brune, 1970, 1971}) \quad (\text{A-10})$$

where R_s is the equivalent circular radius of the rectangular sub-event.

Different values of slip are assigned to each subfault as relative weights so that asperities or non-uniform slip can be incorporated into the methodology. For validation exercises, slip models are taken from the literature and are based on inversions of strong motion as well as regional or teleseismic recordings. To produce slip distributions for future earthquakes, random slip models are generated based on a statistical asperity model with parameters calibrated to the published slip distributions. This approach has been validated by comparing the modeling uncertainty and bias estimates for the Loma Prieta and Whittier Narrows earthquakes using motion at each site averaged over several (30) random slip models to the bias and uncertainty estimates using the published slip model. The results show nearly identical bias and uncertainty estimates suggesting that averaging the motions over random slip models produces as accurate a prediction at a site as a single motion computed using the "true" slip model which is determined from inverting actual recordings.

The rupture velocity is taken as depth independent at a value of 0.8 times the shear-wave velocity, generally at the depth of the dominant slip. This value is based on a number of studies of source rupture processes which also suggest that rupture velocity is non-uniform. To capture the effects of non-uniform rupture velocity, a random component (20%) is added. The radiation pattern is computed for each subfault, a random component added, and the RMS applied to the motions computed at the site.

The ground-motion time history at the receiver is computed by summing the contributions from each subfault associated with the closest Green function, transforming to the frequency domain, and convolving with the Green function spectrum (Equation A-1). The locations of the Green functions are generally taken at center of each subfault for small subfaults or at a maximum separation of about 5 to 10 km for large subfaults. As a final step, the individual contributions associated with each Green function are summed in the frequency domain, multiplied by the RMS radiation pattern, and the resultant power spectrum at the site is computed. The appropriate duration used in the RVT computations for PGA, PGV, and oscillator response is computed by transforming the summed Fourier spectrum into the time domain and computing the 5 to 75% Arias intensity (Ou and Herrmann, 1990).

As with the point-source model, crustal response effects are accommodated through the

amplification factor ($A(f)$) or by using vertically propagating shear waves through a vertically heterogeneous crustal structure. Propagation path damping, through the $Q(f)$ model, is incorporated from each fault element to the site. Near-surface crustal damping is incorporated through the kappa operator (Equation A-1). To model crustal propagation path effects, the raytracing method of Ou and Herrmann (1990) is applied from each subfault to the site.

Time histories may be computed in the process as well by simply adding a phase spectrum appropriate to the subevent earthquake. The phase spectrum can be extracted from a recording made at close distance to an earthquake of a size comparable to that of the subevent (generally M 5.0 to 6.5). Interestingly, the phase spectrum need not be from a recording in the region of interest (Silva et al., 1989). A recording in WNA (Western North America) can effectively be used to simulate motions appropriate to ENA (Eastern North America). Transforming the Fourier spectrum computed at the site into the time domain results in a computed time history which then includes all of the aspects of rupture propagation and source finiteness, as well as region specific propagation path and site effects.

For fixed fault size, mechanism, and moment, the specific source parameters for the finite-fault are slip distribution, location of nucleation point, and site azimuth. The propagation path and site parameters remain identical for both the point- and finite-source models.

Partition and assessment of ground motion variability

An essential requirement of any numerical modeling approach, particularly one which is implemented in the process of defining design ground motions, is a quantitative assessment of prediction accuracy. A desirable approach to achieving this goal is in a manner which lends itself to characterizing the variability associated with model predictions. For a ground motion model, prediction variability is comprised of two components: modeling variability and parametric variability. Modeling variability is a measure of how well the model works (how accurately it predicts ground motions) when specific parameter values are known. Modeling variability is measured by misfits of model predictions to recorded motions through validation exercises and is due to unaccounted for components in the source, path, and site models (i.e. a point-source cannot model the effects of directivity and linear site response cannot accommodate nonlinear effects). Results from a viable range of values for model parameters (i.e., slip distribution, soil profile, G/G_{max} and hysteretic damping curves, etc). Parametric variability is the sensitivity of a model to a viable range of values for model parameters. The total variability, modeling plus parametric, represents the variance associated with the ground motion prediction and, because it is a necessary component in estimating fractile levels, may be regarded as important as median predictions.

Both the modeling and parametric variabilities may have components of randomness and uncertainty. Table A.1 summarizes the four components of total variability in the context of ground motion predictions. Uncertainty is that portion of both modeling and parametric variability which, in principle, can be reduced as additional information becomes available, whereas randomness represents the intrinsic or irreducible component of variability for a given model or parameter. Randomness is that component of variability which is intrinsic or irreducible for a given model. The uncertainty component reflects a lack of knowledge and may

be reduced as more data are analyzed. For example, in the point-source model, stress drop is generally taken to be independent of source mechanism as well as tectonic region and is found to have a standard error of about 0.7 (natural log) for the CEUS (EPRI, 1993). This variation or uncertainty plus randomness in $\Delta\sigma$ results in a variability in ground motion predictions for future earthquakes. If, for example, it is found that normal faulting earthquakes have generally lower stress drops than strike-slip which are, in turn, lower than reverse mechanism earthquakes, perhaps much of the variability in $\Delta\sigma$ may be reduced. In extensional regimes, where normal faulting earthquakes are most likely to occur, this new information may provide a reduction in variability (uncertainty component) for stress drop, say to 0.3 or 0.4 resulting in less ground motion variation due to a lack of knowledge of the mean or median stress drop. There is, however, a component of this stress drop variability which can never be reduced in the context of the Brune model. This is simply due to the heterogeneity of the earthquake dynamics which is not accounted for in the model and results in the randomness component of parametric variability in stress drop. A more sophisticated model may be able to accommodate or model more accurately source dynamics but, perhaps, at the expense of a larger number of parameters and increased parametric uncertainty (i.e. the finite-fault with slip model and nucleation point as unknown parameters for future earthquakes). That is, more complex models typically seek to reduce modeling randomness by more closely modeling physical phenomena. However, such models often require more comprehensive sets of observed data to constrain additional model parameters, which generally leads to increased parametric variability. If the increased parametric variability is primarily in the form of uncertainty, it is possible to reduce total variability, but only at the additional expense of constraining the additional parameters. Therefore, existing knowledge and/or available resources may limit the ability of more complex models to reduce total variability.

The distinction of randomness and uncertainty is model driven and somewhat arbitrary. The allocation is only important in the context of probabilistic seismic hazard analyses as uncertainty is treated as alternative hypotheses in logic trees while randomness is integrated over in the hazard calculation (Cornell, 1968). For example, the uncertainty component in stress drop may be treated by using an N-point approximation to the stress drop distribution and assigning a branch in a logic tree for each stress drop and associated weight. A reasonable three point approximation to a normal distribution is given by weights of 0.2, 0.6, 0.2 for expected 5%, mean, and 95% values of stress drop respectively. If the distribution of uncertainty in stress drop was such that the 5%, mean, and 95% values were 50, 100, and 200 bars respectively, the stress drop branch on a logic tree would have 50, and 200 bars with weights of 0.2 and 100 bars with a weight of 0.6. The randomness component in stress drop variability would then be formally integrated over in the hazard calculation.

Assessment of Modeling Variability

Modeling variability (uncertainty plus randomness) is usually evaluated by comparing response spectra computed from recordings to predicted spectra and is a direct assessment of model accuracy. The modeling variability is defined as the standard error of the residuals of the log of the average horizontal component (or vertical component) response spectra. The residual is defined as the difference of the logarithms of the observed average 5% damped acceleration response spectra and the predicted response spectra. At each period, the residuals

are squared, and summed over the total number of sites for one or all earthquakes modeled. Dividing the resultant sum by the number of sites results in an estimate of the model variance. Any model bias (average offset) that exists may be estimated in the process (Abrahamson et al., 1990; EPRI, 1993) and used to correct (lower) the variance (and to adjust the median as well). In this approach, the modeling variability can be separated into randomness and uncertainty where the bias corrected variability represents randomness and the total variability represents randomness plus uncertainty. The uncertainty is captured in the model bias as this may be reduced in the future by refining the model. The remaining variability (randomness) remains irreducible for this model. In computing the variance and bias estimates only the frequency range between processing filters at each site (minimum of the 2 components) should be used.

Assessment of Parametric Variability

Parametric variability, or the variation in ground motion predictions due to uncertainty and randomness in model parameters is difficult to assess. Formally, it is straight-forward in that a Monte Carlo approach may be used with each parameter randomly sampled about its mean (median) value either individually for sensitivity analyses (Silva, 1992; Roblee et al., 1996) or in combination to estimate the total parametric variability (Silva, 1992; EPRI, 1993). In reality, however, there are two complicating factors.

The first factor involves the specific parameters kept fixed with all earthquakes, paths, and sites when computing the modeling variability. These parameters are then implicitly included in modeling variability provided the data sample a sufficiently wide range in source, path, and site conditions. The parameters which are varied during the assessment of modeling variation should have a degree of uncertainty and randomness associated with them for the next earthquake. Any ground motion prediction should then have a variation reflecting this lack of knowledge and randomness in the free parameters.

An important adjunct to fixed and free parameters is the issue of parameters which may vary but by fixed rules. For example, source rise time (Equation A-8) is magnitude dependent and in the stochastic finite-source model is specified by an empirical relation. In evaluating the modeling variability with different magnitude earthquakes, rise time is varied, but because it follows a strict rule, any variability associated with rise time variation is counted in modeling variability. This is strictly true only if the sample of earthquakes has adequately spanned the space of magnitude, source mechanism, and other factors which may affect rise time. Also, the earthquake to be modeled must be within that validation space. As a result, the validation or assessment of model variation should be done on as large a number of earthquakes of varying sizes and mechanisms as possible.

The second, more obvious factor in assessing parametric variability is a knowledge of the appropriate distributions for the parameters (assuming correct values for median or mean estimates are known). In general, for the stochastic models, median parameter values and uncertainties are based, to the extent possible, on evaluating the parameters derived from previous earthquakes (Silva, 1992; EPRI, 1993).

The parametric variability is site, path, and source dependent and must be evaluated for

each modeling application (Roblee et al., 1996). For example, at large source-to-site distances, crustal path damping may control short-period motions. At close distances to a large fault, both the site and finite-source (asperity location and nucleation point) may dominate, and, depending upon site characteristics, the source or site may control different frequency ranges (Silva, 1992; Roblee et al., 1996). Additionally, level of control motion may affect the relative importance of G/G_{\max} and hysteretic damping curves.

In combining modeling and parametric variations, independence is assumed (covariance is zero) and the variances are simply added to give the total variability.

$$\ln\sigma^2_T = \ln\sigma^2_M + \ln\sigma^2_P \quad (\text{A-11}),$$

where

$\ln\sigma^2_M$ = modeling variation,

$\ln\sigma^2_P$ = parametric variation.

Validation Of The Point- and Finite-Source Models

In a recent Department of Energy sponsored project (Silva et al., 1997), both the point- and finite-source stochastic models were validated in a systematic and comprehensive manner. In this project, 16 well recorded earthquakes were modeled at about 500 sites. Magnitudes ranged from M 5.3 to M 7.4 with fault distances from about 1 km out to 218 km for WUS earthquakes and 460 km for CEUS earthquakes. This range in magnitude and distance as well as number of earthquakes and sites results in the most comprehensively validated model currently available to simulate strong ground motions.

A unique aspect of this validation is that rock and soil sites were modeled using generic rock and soil profiles and equivalent-linear site response. Validations done with other simulation procedures typically neglect site conditions as well as nonlinearity resulting in ambiguity in interpretation of the simulated motions.

Point-Source Model

Final model bias and variability estimates for the point-source model are shown in Figure A1. Over all the sites (Figure A1) the bias is slightly positive for frequencies greater than about 10 Hz and is near zero from about 10 Hz to 1 Hz. Below 1 Hz, a stable point-source

²Strong ground motions are generally considered to be log normally distributed.

overprediction is reflected in the negative bias. The analyses are considered reliable down to about 0.3 Hz (3.3 sec) where the point-source shows about a 40% overprediction.

The model variability is low, about 0.5 above about 3 to 4 Hz and increases with decreasing frequency to near 1 at 0.3 Hz. Above 1 Hz, there is little difference between the total variability (uncertainty plus randomness) and randomness (bias corrected variability) reflecting the near zero bias estimates. Below 1 Hz there is considerable uncertainty contributing to the total variability suggesting that the model can be measurably improved as its predictions tend to be consistently high at very low frequencies (≤ 1 Hz). This stable misfit may be interpreted as the presence of a second corner frequency for WNA sources (Atkinson and Silva, 1997).

Finite-Source Model

For the finite-fault, Figure A2 shows the corresponding bias and variability estimates. For all the sites, the finite-source model provides slightly smaller bias estimates and, surprisingly, slightly higher variability for frequencies exceeding about 5 Hz. The low frequency (≤ 1 Hz) point-source overprediction is not present in the finite-source results, indicating that it is giving more accurate predictions than the point-source model over a broad frequency range, from about 0.3 Hz (the lowest frequency of reliable analyses) to the highest frequency of the analyses.

In general, for frequencies of about 1 Hz and above the point-source and finite-source give comparable results: the bias estimates are small (near zero) and the variabilities range from about 0.5 to 0.6. These estimates are low considering the analyses are based on a data set comprised of earthquakes with M less than M 6.5 (288 of 513 sites) and high frequency ground motion variance decreases with increasing magnitude, particularly above M 6.5 (Youngs et al., 1995) Additionally, for the vast majority of sites, generic site conditions were used (inversion kappa values were used for only the Saguenay and Nahanni earthquake analyses, 25 rock sites). As a result, the model variability (mean = 0) contains the total uncertainty and randomness contribution for the site. The parametric variability due to uncertainty and randomness in site parameters: shear-wave velocity, profile depth, G/G_{max} and hysteretic damping curves need not be added to the model variability estimates. It is useful to perform parametric variations to assess site parameter sensitivities on the ground motions, but only source and path damping $Q(f)$ parametric variabilities require assessment on a site specific basis and added to the model variability. The source uncertainty and randomness components include point-source stress drop and finite-source slip model and nucleation point variations (Silva, 1992).

Empirical Attenuation Model

As an additional assessment of the stochastic models, bias and variability estimates were made over the same earthquakes (except Saguenay since it was not used in the regressions) and sites using a recently develop empirical attenuation relation (Abrahamson and Silva, 1997). For all the sites, the estimates are shown in Figure A3. Interestingly, the point-source overprediction below about 1 Hz is present in the empirical relation perhaps suggesting that this suite of earthquakes possess lower than expected motions in this frequency range as the empirical model

REFERENCES

- Abrahamson, N.A. and W.J. Silva (1997). "Empirical response spectral attenuation relations for shallow crustal earthquakes." *Seismological Research Lett.*, 68(1), 94-127.
- Abrahamson, N.A., P.G. Somerville, and C.A. Cornell (1990). "Uncertainty in numerical strong motion predictions" *Proc. Fourth U.S. Nat. Conf. Earth. Engin.*, Palm Springs, CA., 1, 407-416.
- Aki, K. and P.G. Richards. (1980). "*Quantitative siesmology.*" W. H. Freeman and Co., San Francisco, California.
- Atkinson, G.M and W.J. Silva (1997). "An empirical study of earthquake source spectra for California earthquakes." *Bull. Seism. Soc. Am.* 87(1), 97-113.
- Anderson, J.G. and S.E. Hough (1984). "A Model for the Shape of the Fourier Amplitude Spectrum of Acceleration at High Frequencies." *Bulletin of the Seismological Society of America*, 74(5), 1969-1993.
- Atkinson, G.M. (1984). "Attenuation of strong ground motion in Canada from a random vibrations approach." *Bull. Seism. Soc. Am.*, 74(5), 2629-2653.
- Boore, D.M., W.B. Joyner, and T.E. Fumal (1997). "Equations for estimating horizontal response spectra and peak acceleration from Western North American earthquakes: A summary of recent work." *Seism. Res. Lett.* 68(1), 128-153.
- Boore, D.M., W.B. Joyner, and T.E. Fumal (1994). "Estimation of response spectra and peak accelerations from western North American earthquakes: and interim report. Part 2. *U.S. Geological Survey Open-File Rept.* 94-127.
- Boore, D.M., and G.M. Atkinson (1987). "Stochastic prediction of ground motion and spectral response parameters at hard-rock sites in eastern North America." *Bull. Seism. Soc. Am.*, 77(2), 440-467.
- Boore, D.M. (1986). "Short-period P- and S-wave radiation from large earthquakes: implications for spectral scaling relations." *Bull. Seism. Soc. Am.*, 76(1) 43-64.
- Boore, D.M. and W.B. Joyner (1984). "A note on the use of random vibration theory to predict peak amplitudes of transient signals." *Bull. Seism. Soc. Am.*, 74, 2035-2039.
- Boore, D.M. (1983). "Stochastic simulation of high-frequency ground motions based on seismological models of the radiated spectra." *Bull. Seism. Soc. Am.*, 73(6), 1865-1894.
- Brune, J.N. (1971). "Correction." *J. Geophys. Res.* 76, 5002.

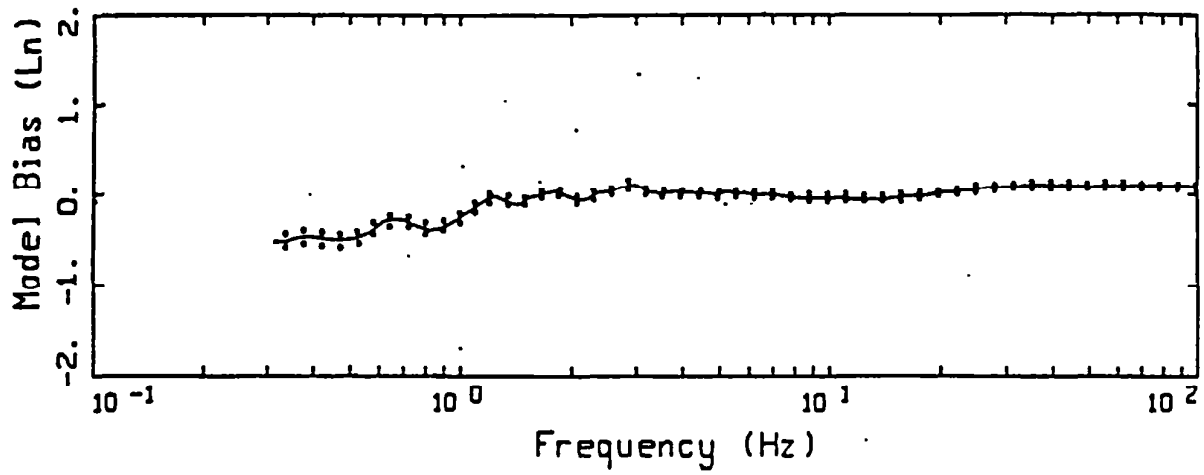
- Brune, J.N. (1970). "Tectonic stress and the spectra of seismic shear waves from earthquakes." *J. Geophys. Res.* 75, 4997-5009.
- Campbell, K.W. (1993) "Empirical prediction of near-source ground motion from large earthquakes." in V.K. Gaur, ed., *Proceedings, Intern'l Workshop on Earthquake Hazard and Large Dams in the Himalya*. INTACH, New Delhi, p. 93-103.
- Cornell, C.A. (1968). "Engineering seismic risk analysis." *Bull. Seism. Soc. Am.*, 58, 1583-1606.
- Electric Power Research Institute (1993). "Guidelines for determining design basis ground motions." Palo Alto, Calif: Electric Power Research Institute, vol. 1-5, EPRI TR-102293.
 vol. 1: Methodology and guidelines for estimating earthquake ground motion in eastern North America.
 vol. 2: Appendices for ground motion estimation.
 vol. 3: Appendices for field investigations.
 vol. 4: Appendices for laboratory investigations.
 vol. 5: Quantification of seismic source effects.
- Hanks, T.C. (1982). " f_{max} ." *Bull. Seism. Soc. Am.*, 72, 1867-1879.
- Hanks, T.C. and R.K. McGuire (1981). "The character of high-frequency strong ground motion." *Bull. Seism. Soc. Am.*, 71(6), 2071-2095.
- Hanks, T.C. and H. Kanamori (1979). "A moment magnitude scale." *J. Geophys. Res.*, 84, 2348-2350.
- Hartzell, S., A. Leeds, A. Frankel, and J. Michael (1996). "Site response for urban Los Angeles using aftershocks of the Northridge earthquake." *Bull. Seism. Soc. Am.*, 86(1B), S168-S192.
- Hartzell, S.H. (1978). "Earthquake aftershocks as Green's functions." *Geophys. Res. Letters*, 5, 1-4.
- Hough, S.E., J.G. Anderson, J. Brune, F. Vernon III, J. Berger, J. Fletcher, L. Haar, T. Hanks, and L. Baker (1988). "Attenuation near Anza, California." *Bull. Seism. Soc. Am.*, 78(2), 672-691.
- Hough, S.E. and J.G. Anderson (1988). "High-Frequency Spectra Observed at Anza, California: Implications for Q Structure." *Bull. Seism. Soc. Am.*, 78(2), 692-707.
- Irikura, K. (1983). "Semi-empirical estimation of strong ground motions during large earthquakes." *Bull. Disaster Prevention Res. Inst.*, Kyoto Univ., 33, 63-104.
- McGuire, R. K., A.M. Becker, and N.C. Donovan (1984). "Spectral Estimates of Seismic Shear Waves." *Bull. Seism. Soc. Am.*, 74(4), 1427-1440.

- Ou, G.B. and R.B. Herrmann (1990). "Estimation theory for strong ground motion." *Seism. Res. Letters*. 61.
- Papageorgiou, A.S. and K. Aki (1983). "A specific barrier model for the quantitative description of inhomogeneous faulting and the prediction of strong ground motion, part I, Description of the model." *Bull. Seism. Soc. Am.*, 73(4), 693-722.
- Roblee, C.J., W.J. Silva, G.R. Toro and N. Abrahamson (1996). "Variability in site-specific seismic ground-motion design predictions." in press.
- Rovelli, A., O. Bonamassa, M. Cocco, M. Di Bona, and S. Mazza (1988). "Scaling laws and spectral parameters of the ground motion in active extensional areas in Italy." *Bull. Seism. Soc. Am.*, 78(2), 530-560.
- Schneider, J.F., W.J. Silva, and C.L. Stark (1993). "Ground motion model for the 1989 M 6.9 Loma Prieta earthquake including effects of source, path and site." *Earthquake Spectra*, 9(2), 251-287.
- Silva, W.J., N. Abrahamson, G. Toro, and C. Costantino (1997). "Description and validation of the stochastic ground motion model." Submitted to Brookhaven National Laboratory, Associated Universities, Inc. Upton, New York.
- Silva, W.J. and R. Darragh (1995). "Engineering characterization of earthquake strong ground motion recorded at rock sites." Palo Alto, Calif:Electric Power Research Institute, TR-102261.
- Silva, W.J. and C.L. Stark (1993) "Source, path, and site ground motion model for the 1989 M 6.9 Loma Prieta earthquake." CDMG draft final report.
- Silva, W.J. (1992). "Factors controlling strong ground motions and their associated uncertainties." *Dynamic Analysis and Design Considerations for High Level Nuclear Waste Repositories*, ASCE 132-161.
- Silva, W.J. (1991). "Global characteristics and site geometry." Chapter 6 in *Proceedings: NSF/EPRI Workshop on Dynamic Soil Properties and Site Characterization*. Palo Alto, Calif.: Electric Power Research Institute, NP-7337.
- Silva, W. J., R. Darragh, C. Stark, I. Wong, J. C. Stepp, J. Schneider, and S-J. Chiou (1990). "A Methodology to Estimate Design Response Spectra in the Near-Source Region of Large Earthquakes Using the Band-Limited-White-Noise Ground Motion Model". *Procee. of the Fourth U.S. Conf. on Earthquake Engineering*, Palm Springs, California. 1, 487-494.
- Silva, W.J., R.B. Darragh, R.K. Green and F.T. Turcotte (1989). *Estimated Ground Motions for a new madrid Event*. U.S. Army Engineer Waterways Experiment Station, Wash., DC, Misc. Paper GL-89-17.

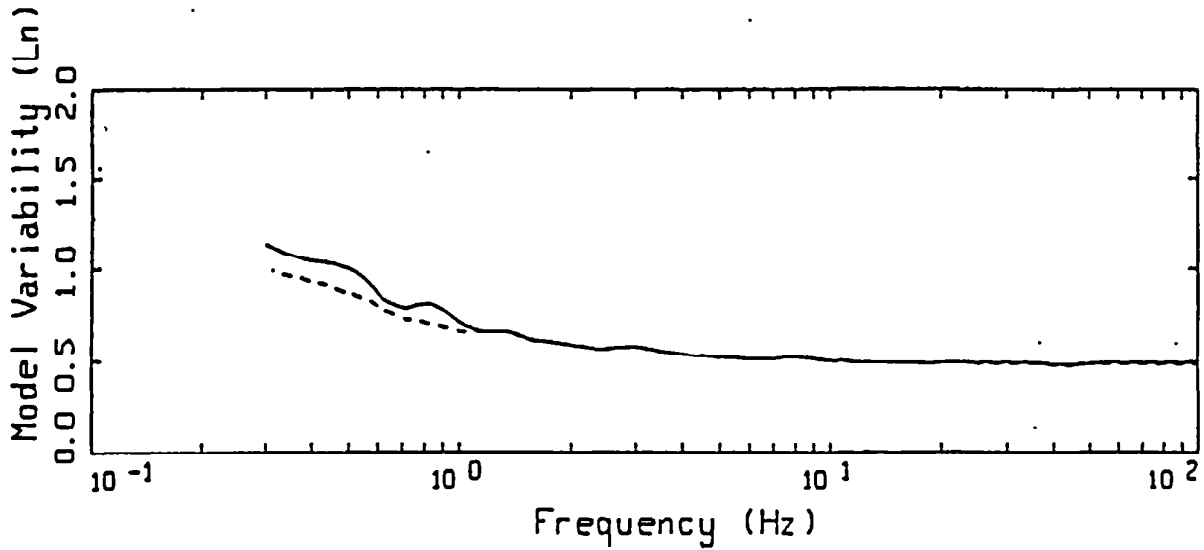
- Silva, W. J. and R. K. Green (1988). "Magnitude and Distance Scaling of Response Spectral Shapes for Rock Sites with Applications to North American Environments." In *Proceedings: Workshop on Estimation of Ground Motion in the Eastern United States*, EPRI NP-5875, Electric Power Research Institute.
- Silva, W. J., T. Turcotte, and Y. Moriwaki (1988). "Soil Response to Earthquake Ground Motion," Electric Power Research Institute, Walnut Creek, California, Report No. NP-5747.
- Silva, W.J. and K. Lee (1987). "WES RASCAL code for synthesizing earthquake ground motions." State-of-the-Art for Assessing Earthquake Hazards in the United States, Report 24, U.S. Army Engineers Waterways Experiment Station, Miscellaneous Paper S-73-1.
- Somerville, P.G., R. Graves and C. Saikia (1995). "TECHNICAL REPORT: Characterization of ground motions during the Northridge earthquake of January 17, 1994." *Structural Engineers Association of California (SEAOC)*. Report No. SAC-95-03.
- Toro, G. R. and R. K. McGuire (1987). "An Investigation into Earthquake Ground Motion Characteristics in Eastern North America." *Bull. Seism. Soc. Am.*, 77(2), 468-489.
- Toro, G. R. (1985). "Stochastic Model Estimates of Strong Ground Motion." In *Seismic Hazard Methodology for Nuclear Facilities in the Eastern United States*, Appendix B, R. K. McGuire, ed., Electric Power Research Institute, Project P101-29.
- Wald, D.J. (1996). "Slip history of the 1995 Kobe, Japan, earthquake determined from strong motion, teleseismic, and geodetic data." *J. of Physics of the Earth*, in press.
- Wald, D.J. and T.H. Heaton (1994). "Spatial and temporal distribution of slip for the 1992 Landers, California, earthquake." *Bull. Seism. Soc. Amer.*, 84(3), 668-691.
- Wells, D.L. and K.J. Coppersmith (1994). "New empirical relationships among magnitude, rupture length, rupture width, rupture area, and surface displacement." *Bull. Seism. Soc. Am.* 84(4), 974-1002.
- Youngs, R.R., N.A. Abrahamson, F. Makdisi, and K. Sadigh (1995). "Magnitude dependent dispersion in peak ground acceleration." *Bull. Seism. Soc. Amer.*, 85(1), 161-1, 176.

Table A.1		
CONTRIBUTIONS TO TOTAL VARIABILITY IN GROUND MOTION MODELS		
	Modeling Variability	Parametric Variability
Uncertainty <i>(also Epistemic Uncertainty)</i>	<u>Modeling Uncertainty:</u> Variability in predicted motions resulting from particular model assumptions, simplifications and/or fixed parameter values. <i>Can be reduced by adjusting or "calibrating" model to better fit observed earthquake response.</i>	<u>Parametric Uncertainty:</u> Variability in predicted motions resulting from incomplete data needed to characterize parameters. <i>Can be reduced by collection of additional information which better constrains parameters</i>
Randomness <i>(also Aleatory Uncertainty)</i>	<u>Modeling Randomness:</u> Variability in predicted motions resulting from discrepancies between model and actual complex physical processes. <i>Cannot be reduced for a given model form.</i>	<u>Parametric Randomness:</u> Variability in predicted motions resulting from inherent randomness of parameter values. <i>Cannot be reduced a priori*** by collection of additional information.</i>

***Some parameters (e.g. source characteristics) may be well defined after an earthquakes.



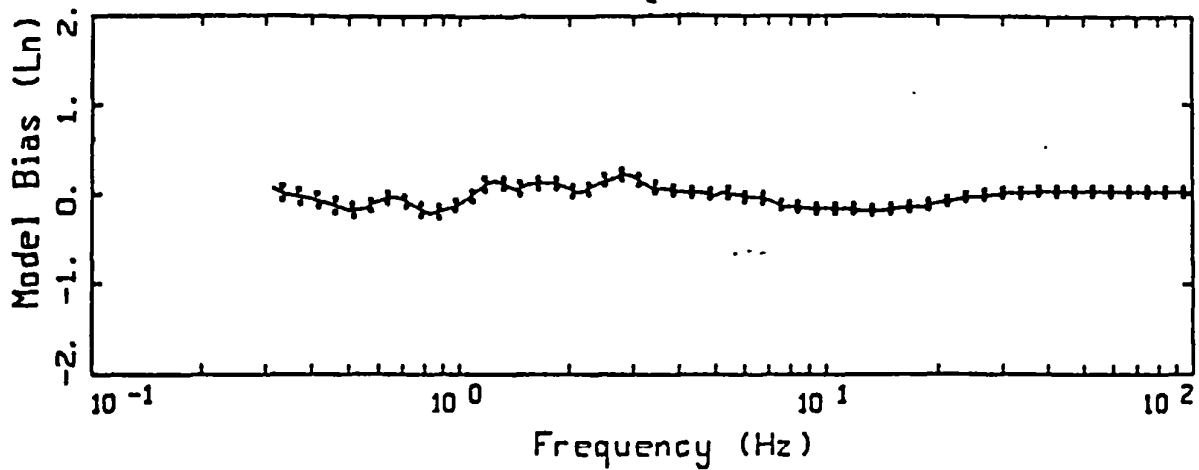
LEGEND
 — MODELING BIAS
 90% CONFIDENCE INTERVAL OF MODELING BIAS
 90% CONFIDENCE INTERVAL OF MODELING BIAS



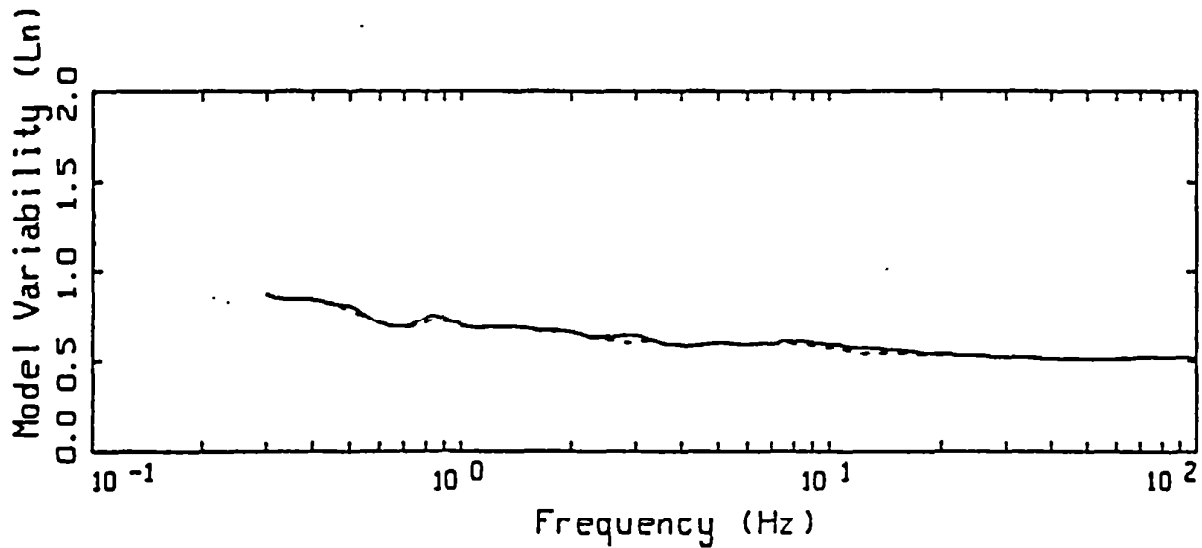
LEGEND
 — MEAN=0.0
 - - - - BIAS CORRECTED

16 EARTHQUAKES POINT-SOURCE
 NONLINEAR, ALL 503 SITES

Figure A1. Model bias and variability estimates for all earthquakes computed over all 503 sites for the point-source model.



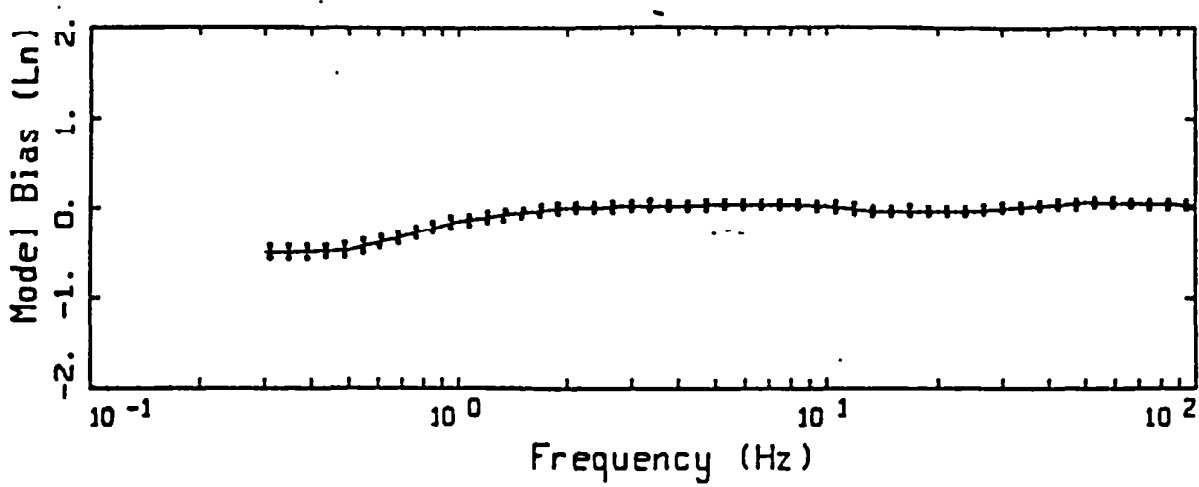
LEGEND
 — MODELING BIAS
 90% CONFIDENCE INTERVAL OF MODELING BIAS
 90% CONFIDENCE INTERVAL OF MODELING BIAS



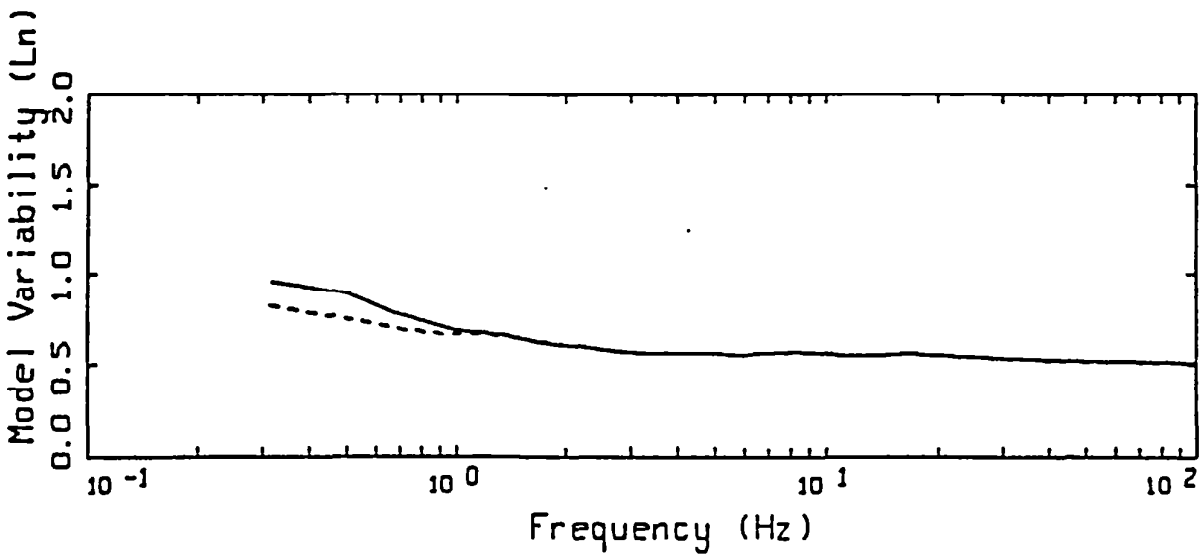
LEGEND
 — MEAN=0.0
 - - - - - BIAS CORRECTED

15 EARTHQUAKES FINITE-SOURCE
 NONLINEAR, ALL 487 SITES

Figure A2. Model bias and variability estimates for all earthquakes computed over all 487 sites for the finite-source model.



LEGEND
 — MODELING BIAS
 90% CONFIDENCE INTERVAL OF MODELING BIAS
 90% CONFIDENCE INTERVAL OF MODELING BIAS



LEGEND
 — MEAN=0.0
 - - - - BIAS CORRECTED

15 EARTHQUAKES, EMPIRICAL RELATION
 ALL 481 SITES

Figure A3. Model bias and variability estimates for all earthquakes computed over all 481 sites for the empirical model.

APPENDIX B

SITE RESPONSE ANALYSIS METHOD

Development of Site Specific Soil Motions

The conventional approach to estimating the effects of site specific site conditions on strong ground motions involves development of a set (1, 2, or 3 component) of time histories compatible with the specified outcrop response spectra to serve as control (or input) motions. The control motions are then used to drive a nonlinear computational formulation to transmit the motions through the profile. Simplified analyses generally assume vertically propagating shear-waves for horizontal components and vertically propagating compression-waves for vertical motions. These are termed one-dimensional site response analyses.

Equivalent-Linear Computational Scheme

The computational scheme which has been most widely employed to evaluate one-dimensional site response assumes vertically-propagating plane shear-waves. Departures of soil response from a linear constitutive relation are treated in an approximate manner through the use of the equivalent-linear approach.

The equivalent-linear approach, in its present form, was introduced by Seed and Idriss (1970). This scheme is a particular application of the general equivalent-linear theory developed by Iwan (1967). Basically, the approach is to approximate a second order nonlinear equation, over a limited range of its variables, by a linear equation. Formally this is done in such a way that the average of the difference between the two systems is minimized. This was done in an ad-hoc manner for ground response modeling by defining an effective strain which is assumed to exist for the duration of the excitation. This value is usually taken as 65% of the peak time-domain strain calculated at the midpoint of each layer, using a linear analysis. Modulus reduction and hysteretic damping curves are then used to define new parameters for each layer based on the effective strain computations. The linear response calculation is repeated, new effective strains evaluated, and iterations performed until the changes in parameters are below some tolerance level. Generally a few iterations are sufficient to achieve a strain-compatible linear solution.

This stepwise analysis procedure was formalized into a one-dimensional, vertically propagating shear-wave code called SHAKE (Schnabel et al., 1972). Subsequently, this code has easily become the most widely used analysis package for one-dimensional site response calculations.

The advantages of the equivalent-linear approach are that parameterization of complex nonlinear soil models is avoided and the mathematical simplicity of a linear analysis is preserved. A truly nonlinear approach requires the specification of the shapes of hysteresis curves and their cyclic dependencies through an increased number of material parameters. In

the equivalent-linear methodology the soil data are utilized directly and, because at each iteration the problem is linear and the material properties are frequency independent, the damping is rate independent and hysteresis loops close.

Careful validation exercises between equivalent-linear and fully nonlinear formulations using recorded motions from 0.05 to 0.50g showed little difference in results (EPRI, 1993). Both formulations compared very favorably to recorded motions suggesting both the adequacy of the vertically propagating shear-wave model and the approximate equivalent-linear formulation. While the assumptions of vertically propagating shear-waves and equivalent-linear soil response certainly represent approximations to actual conditions, their combination has achieved demonstrated success in modeling observations of site effects and represent a stable, mature, and reliable means of estimating the effects of site conditions on strong ground motions (Schnabel et al., 1972; Silva et al., 1988; Schneider et al., 1993; EPRI, 1993).

To accommodate both uncertainty and randomness in dynamic material properties, analyses are typically done for the best estimate shear-wave velocity profile as well as upper- and lower-range profiles. The upper- and lower-ranges are usually specified as twice and one-half the best estimate shear-wave moduli. Depending upon the nature of the structure, the final design spectrum is then based upon an envelope or average of the three spectra.

For vertical motions, the SHAKE code is also used with compression-wave velocities and damping substituted for the shear-wave values. To accommodate possible nonlinear response on the vertical component, since modulus reduction and hysteretic damping curves are not generally available for the constrained modulus, the low-strain Poisson's ratio is usually fixed and strain compatible compression-wave velocities calculated using the strain compatible shear moduli from the horizontal component analyses combined with the low-strain Poisson's ratios. In a similar manner, strain compatible compression-wave damping values are estimated by combining the strain compatible shear-wave damping values with the low-strain damping in bulk or pure volume change. This process assumes the loss in bulk (volume change) is constant or strain independent. Alternatively, zero loss in bulk is assumed and the equation relating shear- and compression-wave damping (η_s and η_p) and velocities (V_s and V_p)

$$\eta_p \approx \frac{4}{3} \frac{V_s}{V_p} \eta_s , \quad (\text{B-1})$$

is used.

RVT Based Computational Scheme

The computational scheme employed to compute the site response for this project uses an alternative approach employing random vibration theory (RVT). In this approach the control motion power spectrum is propagated through the one-dimensional soil profile using the plane-

wave propagators of Silva (1976). In this formulation only SH waves are considered. Arbitrary angles of incidence may be specified but normal incidence is used throughout the present analyses.

In order to treat possible material nonlinearities, an RVT based equivalent-linear formulation is employed. Random process theory is used to predict peak time domain values of shear-strain based upon the shear-strain power spectrum. In this sense the procedure is analogous to the program SHAKE except that peak shear-strains in SHAKE are measured in the time domain. The purely frequency domain approach obviates a time domain control motion and, perhaps just as significant, eliminates the need for a suite of analyses based on different input motions. This arises because each time domain analysis may be viewed as one realization of a random process. Different control motion time histories reflecting different time domain characteristics but with nearly identical response spectra can result in different nonlinear and equivalent-linear response.

In this case, several realizations of the random process must be sampled to have a statistically stable estimate of site response. The realizations are usually performed by employing different control motions with approximately the same level of peak accelerations and response spectra.

In the case of the frequency domain approach, the estimates of peak shear-strain as well as oscillator response are, as a result of the random process theory, fundamentally probabilistic in nature. For fixed material properties, stable estimates of site response can then be obtained with a single run.

In the context of the RVT equivalent-linear approach, a more robust method of incorporating uncertainty and randomness of dynamic material properties into the computed response has been developed. Because analyses with multiple time histories are not required, parametric variability can be accurately assessed through a Monte Carlo approach by randomly varying dynamic material properties. This results in median as well as other fractile levels (e.g. 16th, mean, 84th) of smooth response spectra at the surface of the site. The availability of fractile levels reflecting randomness and uncertainty in dynamic material properties then permits a more rational basis for selecting levels of risk.

In order to randomly vary the shear-wave velocity profile, a profile randomization scheme has been developed which varies both layer velocity and thickness. The randomization is based on a correlation model developed from an analysis of variance on about 500 measured shear-wave velocity profiles (EPRI, 1993; Silva et al., 1997). Profile depth (depth to competent material) is also varied on a site specific basis using a uniform distribution. The depth range is generally selected to reflect expected variability over the structural foundation as well as uncertainty in the estimation of depth to competent material.

To model parametric variability for compression-waves, the base-case Poisson's ratio is generally fixed. Suites of compatible random compression- and shear-wave velocities are then generated based on the random shear-wave velocities profiles.

To accommodate variability in modulus reduction and hysteretic damping curves on a generic basis, the curves are independently randomized about the base case values. A log normal distribution is assumed with a σ_{\ln} of 0.35 at a cyclic shear strain of $3 \times 10^{-2}\%$. These values are based on an analysis of variance on a suite of laboratory test results. An upper and lower bound truncation of 2σ is used to prevent modulus reduction or damping models that are not physically possible. The random curves are generated by sampling the transformed normal distribution with a σ_{\ln} of 0.35, computing the change in normalized modulus reduction or percent damping at $3 \times 10^{-2}\%$ shear strain, and applying this factor at all strains. The random perturbation factor is reduced or tapered near the ends of the strain range to preserve the general shape of the median curves (Silva, 1992).

To model vertical motions, incident inclined compression- and shear (SV)-waves and assumed. Raytracing is done from the source location to the site to obtain appropriate angles of incidence. In the P-SV site response analyses, linear response is assumed in both compression and shear with the low-strain shear-wave damping used for the compression-wave damping (Johnson and Silva, 1981). The vertical and horizontal motions are treated independently in separate analyses. Validation exercises with a fully 3-D soil model using recorded motions up to 0.50%g showed these approximations to be validate (EPRI, 1993).

In addition, the site response model for the vertical motions has been validated at over 100 rock and soil sites for three large earthquakes: 1989 M 6.9 Loma Prieta, 1992 M 7.2 Landers, and the 1994 Northridge earthquakes. In general, the model performs well and captures the site and distance dependency of vertical motions over the frequency range of about 0.3 to 50.0 Hz and the fault distance range of about 1 to 100 km.

REFERENCES

- Electric Power Research Institute (1993). "Guidelines for determining design basis ground motions." Palo Alto, Calif: Electric Power Research Institute, vol. 1-5, EPRI TR-102293.
vol. 1: Methodology and guidelines for estimating earthquake ground motion in eastern North America.
vol. 2: Appendices for ground motion estimation.
vol. 3: Appendices for field investigations.
vol. 4: Appendices for laboratory investigations.
vol. 5: Quantification of seismic source effects.
- Iwan, W.D. (1967). "On a class of models for the yielding behavior of continuous and composite systems." *J. Appl. Mech.*, 34, 612-617.
- Johnson, L.R. and W.J. Silva (1981). "The effects of unconsolidated sediments upon the ground motion during local earthquakes." *Bull. Seism. Soc. Am.*, 71, 127-142.
- Schnabel, P.B., J. Lysmer, and H.B. Seed (1972). *SHAKE: a Computer Program for Earthquake Response Analysis of Horizontally Layered Sites*. Earthq. Engin. Res. Center, Univ. of Calif. at Berkeley, EERC 72-12.
- Schneider, J.F., W.J. Silva, and C.L. Stark (1993). Ground motion model for the 1989 M 6.9 Loma Prieta earthquake including effects of source, path and site. *Earthquake Spectra*, 9(2), 251-287.
- Seed, H.B. and I.M. Idriss (1970). "Soil Moduli and Damping Factors for Dynamic Response Analyses," Earthq. Eng. Res. Center, Univ. of Calif. at Berkeley, Report No. UCB/EERC-70/10.
- Silva, W.J., N. Abrahamson, G. Toro, and C. Costantino (1997). "Description and validation of the stochastic ground motion model." Submitted to Brookhaven National Laboratory, Associated Universities, Inc. Upton, New York.
- Silva, W.J. (1992). "Factors controlling strong ground motions and their associated uncertainties." *Dynamic Analysis and Design Considerations for High Level Nuclear Waste Repositories*, ASCE 132-161.
- Silva, W. J., T. Turcotte, and Y. Moriwaki, (1988). "Soil Response to Earthquake Ground Motion," Electric Power Research Institute, Walnut Creek, California, Report No. NP-5747.
- Silva, W.J. (1976). "Body Waves in a Layered Anelastic solid." *Bull. Seis. Soc. Am.*, vol. 66(5), 1539-1554.

